J. Fluid Mech. (1982), *vol.* 124, *pp.* 139–172
Printed in Great Britain

Acoustic streaming in swirling flow and the Ranque–Hilsch (vortex-tube) effect

By M. KUROSAKA

The University of Tennessee Space Institute,
Tullahoma, Tennessee 37388

(Received 24 September 1981 and in revised form 11 March 1982)

The Ranque–Hilsch effect, observed in swirling flow within a single tube, is a spontaneous separation of total temperature, with the colder stream near the tube centreline and the hotter air near its periphery. Despite its simplicity, the mechanism of the Ranque–Hilsch effect has been a matter of long-standing dispute. Here we demonstrate, through analysis and experiment, that the acoustic streaming induced by orderly disturbances within the swirling flow is, to a substantial degree, a cause of the Ranque–Hilsch effect. The analysis predicts that the streaming induced by the pure tone, a spinning wave corresponding to the first tangential mode, deforms the base Rankine vortex into a forced vortex, resulting in total temperature separation in the radial direction. This is confirmed by experiments, where, in the Ranque–Hilsch tube of uniflow arrangement, we install acoustic suppressors of organ-pipe type, tuned to the discrete frequency of the first tangential mode, attenuate its amplitude, and show that this does indeed reduce the total temperature separation.

1. Introduction

The subject of acoustic streaming owes its origin to Lord Rayleigh (1884); led by Faraday's observation (1831) and the patterns in the Kundt tube, he showed that sound waves can and do generate a steady current through the action of Reynolds stresses, induced near the solid boundary by the periodic disturbances themselves. For a modern review of the subject in general we refer to Lighthill (1978*a*).

As yet, however, with the possible exception of Secomb (1978), the studies of streaming appear to have been subject to a common restriction that the fluid be initially in a state of rest.

In this paper we shall treat an acoustic-streaming problem which, by contrast, depends crucially on the motion of a gas. To be specific, *for a swirling gas within a cylindrical duct, we submit that the acoustic streaming of the gas with swirl produces the Ranque–Hilsch effect: the radial separation of total temperature.* Although it has generally – and often vaguely – been accepted that some form of unsteadiness is needed to interpret this perplexing phenomenon, the key to the explanation is precisely this unforeseen mechanism of acoustic streaming, which is induced by *orderly, periodic disturbances* within swirling flows. We shall first demonstrate this analytically, and then confirm it experimentally. But, first, a discussion on the background is in order.

Several years ago a striking phenomenon, with unusual features, accidentally revealed itself in a swirling-flow test rig called an annular cascade (Danforth 1977,

private communication; Rakowski, Ellis & Bankhead 1978; Rakowski & Ellis 1978). The whole apparatus was stationary and in the shape of an annular conduit formed between inner and outer casings; therein, air, having been made to swirl by vanes, spiralled aft. A check-out test of the rig immediately disclosed the presence of a loud whistle, a pure tone, the level of which rose to a deafening intensity of 180 dB. The occurrence of this ear-splitting sound was all the more remarkable since, for one thing, none of the components of the rig was rotating; only air was in swirling motion. For another, the sound occurred even before the installation of a test cascade; except for the swirl vanes, nothing lay in the way of the flow path. Its discrete frequency increased almost proportionately to swirl, from 350 to 500 Hz; the dynamic disturbance was spinning circumferentially with the first tangential mode, accompanied by higher harmonics.

Most surprising of all, *this intense pure tone in swirling flow induced a marked distortion to the steady-state or the time-averaged components of the flow field – its 'd.c.' parts.* Accompanied by an increasingly louder whistle, the tangential velocity near the inner wall became, above a certain level, abruptly reduced to a considerable extent; the radial profile, which had remained a free-vortex type (as it was designed to be), metamorphosed into one somewhat akin to a forced vortex. At the same time the total temperature, initially uniform at the inlet and equal to 36 °C, spontaneously separated into a hotter stream of about 48 °C near the outer wall and a colder one of 28 °C near the inner wall, with a radial difference equal to 20 °C – strongly reminiscent of the Ranque–Hilsch effect.

Because of the severity of these dynamic fluctuations, which posed a serious threat to the original purpose of the rig, the inner and outer walls were provided with tuned acoustic suppressors; this did remove the unacceptable dynamic flow disturbances.

Now that the unsteady fluctuations had been eliminated, what happened to the profiles of steady flow? The answer was *that the distortion in the velocity and temperature distribution vanished. The Ranque–Hilsch effect had gone.*

Acoustic streaming appears to have somehow deformed the steady flow field, both in velocity and temperature, and if so, then this phenomenon of arresting interest affords a singular insight into the mechanism of little-understood Ranque–Hilsch effects, which we shall discuss briefly below.

We recall that in the Ranque–Hilsch tube (Ranque 1933; Hilsch 1947) or the vortex tube, compressed air enters a single straight tube through tangential injection nozzles. Once within the tube, the swirling air segregates by itself into two streams of different total temperature: the hotter air near the periphery of the tube and the colder air at the centreline, a separation effect already mentioned with regard to the annular cascade. In the conventional counterflow Ranque–Hilsch tube, the cold air is extracted from an orifice located near the inlet, and the hot air escapes from the other end. Even by closing the cold orifice, however, the air flowing in only one direction can still produce the radial separation of total temperature; this, called the uniflow type, will be adopted later for our analysis and experiment because of the simpler flow pattern.

Although the existence of total-temperature separation in Ranque–Hilsch tubes is beyond any doubt, none of the theoretical explanations so far devised appears to have found unreserved acceptance. For example, the oft-cited turbulent-migration theory (Van Deemter 1952; Deissler & Perlmutter 1960; Linderstrøm-Lang 1971)

fails to explain why the purported random radial migration of fluid lumps does not separate the total temperature in other swirling-flow apparatuses, which are equally turbulent and provided with the same tangential injection as the one for the Ranque–Hilsch tube; for example compare figure 3 of Batson & Sforzini (1970) with figure 4 of Hartnett & Eckert (1957). The other theories (Schepper 1951; Sibulkin 1962) appear to be open to equally serious objections.

The experimental evidence mentioned on the annular cascade compels us to turn towards acoustic streaming as an agent of the Ranque–Hilsch effect – the acoustic streaming induced through the Reynolds stresses that are caused by organized periodic disturbances rather than by stochastic, random motion.

In the literature on the Ranque–Hilsch tube, allusions to the presence of intense periodic disturbances abound. Hilsch (1947), McGee (1950), Savino & Ragsdale (1961), Ragsdale (1961) and Kendall (1962) noted the disturbances of pure-tone type, whistle or scream. In fact, Savino & Ragsdale (1961) recounted an incident where a loud screaming noise was accompanied by 6–11 °C change in total temperature, a phenomenon evocative of that experienced with the annular cascade. None of them, however, proceeded beyond the stage of making passing observations on it.

To a certain extent, the work of Sprenger (1951) foreshadows ours in its spirit. In the Ranque–Hilsch tube with its hot end closed and only its cold end open, he measured periodic disturbances by spreading lycopodium to form a Kundt pattern. However, the pattern was apparently used to measure only the wavelength of discrete disturbances, since he did not pin the Ranque–Hilsch effect down to any explicit mechanism. Rather, by appealing to the analogy of the resonance tube, he later simply suggested (Sprenger 1954) that the organized unsteadiness† might produce the energy separation. More to the point is the highly suggestive circumstance that led to the discovery of the vortex whistle by Vonnegut (1954). While engaged in experiments exploring the application of the Ranque–Hilsch cooling effect, Vonnegut (1950) had observed the presence of a pure-tone noise. Although he did not connect it with a mechanism of the Ranque–Hilsch effect, from this hint he constructed a musical instrument – the so-called 'vortex whistle' – where air, injected tangentially into a cylinder, swirls into a tube of smaller diameter. The sound thus emitted was found to have a discrete frequency proportional to flow rate. We recall that the frequency of the pure-tone noise in the similar swirling flow within the annular cascade was also proportional to the Mach number.

With the preceding background description in mind, we go right to the heart of the present theory: *acoustic streaming by the vortex whistle produces the Ranque–Hilsch effect.*

Here we redefine the vortex whistle in a broader sense as the pure-tone noise existing in any swirling flow, whether the fluid is contained within a single pipe or an annular duct; it is characterized by a spiralling waveform such as $\cos(m\theta + kz - \omega t)$, where θ and z are the circumferential and axial coordinates respectively, m and k are the corresponding wavenumbers and t is the time. ω is a *discrete* fundamental frequency determined uniquely for given values of m, k, swirl and the axial velocity.

The fact that the rotating fluid is endowed with a capacity to support such a spinning wave motion has long been established (e.g. Kelvin 1880; Greenspan 1968);

† Syred & Beér (1972) also recorded regular sinusoidal fluctuations in the tube and suggested their possible connection with the energy separation.

like other pure-tone noise in flow, the vortex whistle, latent in swirling flow, emerges out of the selective amplification of background disturbances. This pure tone, we submit, brings the total-temperature separation into being.

Now this is not to suggest that the flow in the Ranque–Hilsch tube remains laminar; it is turbulent. But we shall argue and later verify experimentally (figure 5) that in the frequency spectrum, over and above turbulence, there soars a prominent peak of the vortex whistle possessing the discrete frequency ω. This organized disturbance dwarfs the random fluctuation, rendering the latter negligible by comparison. For a model problem of the Ranque–Hilsch tube posed as such, the frequency of the pure tone determined from the linearized inviscid solution will be found to increase proportionately to swirl. More important, ω, *thus calculated by neglecting the random components of disturbances, does agree closely with the measurement of the vortex whistle* (figure 6), with $m = 1$, the first tangential mode.

From this linearized treatment we proceed to the second-order analysis in order to calculate streaming; this is, of course, the temporal average of nonlinear terms or products between linear waves like $\cos^2(m\theta + kz - \omega t)$, whose time-dependent parts take the form $\cos(2m\theta + 2kz - 2\omega t)$ – an induced, spiralling wave with its frequency and wavenumbers twice those of the vortex whistle.

Concerning this *unsteady* part of the nonlinear terms, we confirm experimentally that such *a second harmonic precisely in the above form is conspicuously in evidence in the data obtained from the Ranque–Hilsch tube*. Its pre-eminence attests, and favours, the anticipated existence of its steady counterpart, or acoustic streaming, which the second harmonics must always keep in tow.

Concerning the *steady* part of the nonlinear terms or acoustic streaming, we shall obtain its expression near a cylindrical surface in general form (equation (22)) applicable to any swirl, and not limited to the one in a single pipe of the Ranque–Hilsch tube. We regard this as the centrepiece of the analytical results.

Applied to a model problem of the Ranque–Hilsch tube, where the base swirl initially imposed is assumed to be a Rankine vortex, the substitution of the calculated frequency ω of the vortex whistle into the above expression reveals the following: the tangential streaming near the tube periphery is always in the same direction as the steady swirl. Thus the streaming adds to the base swirl, and the total d.c. component of swirl near the tube periphery grows in magnitude. This is particularly so at lower tangential modes, since, as m decreases, the tangential streaming grows increasingly larger. This deforms the initial Rankine vortex, and a transition towards a forced vortex is now set in motion. The flow with the initially uniform total temperature becomes separated radially into a hotter gas near the tube periphery and a colder one near the centre. *The Ranque–Hilsch effect now takes shape.*

As mentioned, the vortex whistle in the Ranque–Hilsch tube turns out to be that corresponding to the first tangential mode, with $m = 1$. The pivotal point that this wave does cause the temperature separation, indicated by the theory, will be confirmed by the following test. On the Ranque–Hilsch tube, we install acoustic suppressors of the organ-pipe type (figure 7), tunable to the fundamental frequency ω of the vortex whistle, which corresponds to the first tangential mode, $m = 1$. *We thus attenuate the intensity of the vortex whistle at a tuned frequency, confirm that this induces the reduction of its second harmonic and, most important, verify that this does indeed reduce the total-temperature separation.* Figures 9–13 in § 5.2 display such results. For

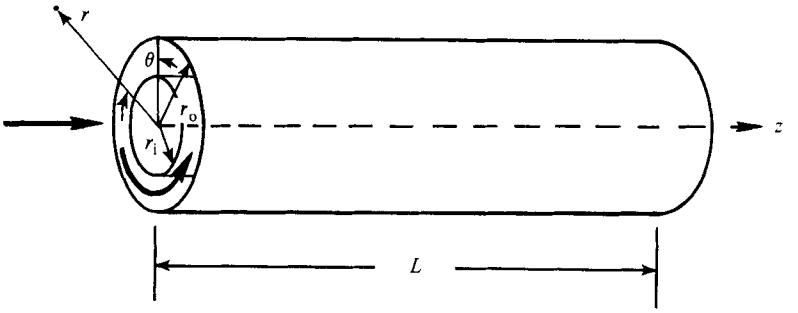

FIGURE 1. Definition sketch.

instance, in figure 9 the acoustic suppressor was tuned to 4·0 kHz; at the moment when the fundamental frequency of the vortex whistle reached the tuned frequency, its level plummeted abruptly by 25 dB, which in turn reduced its second harmonic by 14 dB. At this instant, the cold temperature at the tube centreline, which had gone down as low as −35 °C, immediately jumped to 0·6 °C – with a temperature rise equal to 35·6 °C. These results, more than anything else, seem to validate the heart of the present thesis. (Some readers may prefer to pass directly to § 5, which presents such results.)

2. Statement of the problem

Although our present investigation centres on a single pipe, here we formulate, in anticipation of future work on co-axial cylinders, the following general problem: acoustic streaming in either a single pipe or an annular duct between two circular cylinders. The latter case is sketched in figure 1, where r_0 denotes the radius of the outer cylinder, r_i that of the inner cylinder. For a single pipe, corresponding to the Ranque–Hilsch tube of uniflow type, r_0 still denotes the radius of the cylinder. The fluid is compressible and taken as a perfect gas. We assume that throughout the entire duct length L of interest, the two steady boundary layers formed over the cylinder surfaces are thin; in the inviscid annular region bounded and contained by them, both the circumferential and axial velocities are the predominant components of steady flow, as shown in figure 1. Superimposed upon this steady flow are the fully three-dimensional unsteady disturbances, whose streaming effects we are interested in.

Acoustic streaming is of course an induced steady or added d.c. component. As such, we have to distinguish it from the base steady flow initially imposed before the disturbances are set up. For brevity we henceforth refer to the latter simply as the steady part. Thus the flow at any point consists of three parts: the steady part, the a.c. components of the unsteady disturbances, and their d.c. components or streaming. The sum of the steady part and streaming is the total d.c. component.

For symbols, we use the following: (r, θ, z) are cylindrical coordinates with the corresponding velocity $\mathbf{q} = (u, v, w)$; p is the pressure, ρ the density, T the temperature, μ the coefficient of viscosity, $\nu = \mu/\rho$, Pr the Prandtl number, γ the ratio of specific heats; it turns out, to the order in which we are interested, that the second coefficient of viscosity does not appear. Both the specific heat c_p and Pr are taken, as usual, to be constant; the viscosity law is

$$\mu = \mu(T). \tag{1}$$

The boundary condition on the cylindrical surfaces is $\mathbf{q} = 0$. The thermal condition depends, in general, on the details of unsteady heat transfer through a wall. For simplicity, we assume that either the wall temperature is maintained constant or the walls are insulated.

We first consider the steady part of the flow field. We assume that the steady flow is axisymmetric, and apply the standard outer and inner expansion (Van Dyke 1962*a*, *b*) in negative half-powers of the Reynolds number; we denote the leading term of the outer expansion or the inviscid flow by subscript 0.

As usual, the matching yields $u_0 = 0$ on the walls, and henceforth we are interested in the case where

$$u_0 = 0, \tag{2}$$

at any point of the outer or inviscid region. The rest of the leading terms of the outer expansion or inviscid flow are all taken to be functions of r only, independent of z (and of θ), in view of the assumption of thin boundary layers. Then the only non-trivial component of the equation of motion is the radial equilibrium

$$\rho_0 \frac{v_0^2}{r} = \frac{dp_0}{dr}. \tag{3}$$

For the energy equation, we assume that the leading term of the outer expansion of entropy remains constant everywhere.

The leading terms of the inner expansion of the steady part constitute of course the conventional compressible steady boundary-layer equations. On both cylindrical surfaces, the boundary layers are rotationally symmetric and develop in the z-direction. Their structures are complicated by the presence of two components of the inviscid stream: swirl and axial velocity. However, as shown later, insofar as we limit our attention to the leading term of acoustic streaming at large Reynolds number, the details of the steady boundary layer need not be worked out.

3. Small parameters and expansion series

We now turn to the unsteady disturbances, upon which our emphasis lies. In an effort to seek a tractable ingress to the problem, we assume that the a.c. components of the disturbances are organized, regular and endowed with a fundamental frequency ω; in comparison with them, we neglect the stochastic part of the disturbances according to the discussion of §1.

Now the only known analytical method of obtaining streaming is to resort to the use of an expansion scheme. To pave the way for the selection of the relevant small parameters, consider the linearized inviscid unsteady disturbances. Neglecting the second-order terms, from the set of equations (16*a–g*) in §4.1 we immediately recognize a fact of crucial importance: once a factor $\exp(im\theta + ikz - i\omega t)$ is separated from the amplitudes of the disturbances, the frequency ω does not appear by itself, but arises exclusively in the modified form of

$$-\omega + m\frac{v_0(r)}{r} + kw_0(r) = f(r). \tag{4}$$

This is only to be expected, because it embodies the Doppler shift caused by the steady inviscid swirl v_0 and the axial velocity w_0. Note that the shift is dependent upon the radial position.

In order to obtain acoustic streaming, these inviscid linear waves are to be imposed as external excitations upon the viscous flow near the walls; therefore, in forming a parameter containing a frequency, the relevant one is not the bare ω, but the above f evaluated at the cylindrical surface.

Henceforth, the leading term of the outer expansion of the steady flow, evaluated at R (the radius of the cylinder surface under study) is denoted by subscript e – the 'external' flow at the outer edge of the steady boundary layer; for instance

$$v_e = v_0(R), \quad w_e = w_0(R).$$

Then the appropriate frequency parameter relevant to the acoustic streaming near R is given by

$$\alpha = \tilde{v}_e / f_e R, \tag{5a}$$

where

$$f_e = -\omega + m\frac{v_e}{R} + kw_e, \tag{5b}$$

and $\tilde{v}_e$ is a measure of the *unsteady* disturbance, taken specifically as the amplitude of the linearized inviscid fluctuation (the 'external' unsteady flow) in the circumferential direction, evaluated at the outer edge of the *unsteady* boundary layer.

With respect to the lengthscale, in the problem at hand, three characteristic lengths distinguish themselves: the radius R of the cylinder, the unsteady-boundary-layer thickness $\delta_u = [\nu_e/|f_e|]^{\frac{1}{2}}$, and the steady-boundary-layer thickness $\delta = LRe^{-\frac{1}{2}}$, where Re is the Reynolds number based upon L. From the three lengths, we form two additional parameters β and ϵ, defined by

$$\beta \equiv \frac{\delta_u}{R} = \left[\frac{\nu_e}{|f_e|}\right]^{\frac{1}{2}} \frac{1}{R}, \tag{6}$$

$$\epsilon \equiv \frac{\delta}{\delta_u} = \frac{L}{\beta R\, Re^{\frac{1}{2}}}. \tag{7}$$

As regards δ_u and β, the absolute value of f_e is needed in the above; for, as seen from (5b), its sign can and does switch, depending upon the relative magnitudes of ω, v_e and w_e. Note that as the steady flow varies the unsteady-boundary-layer thickness δ_u can change, even for a given frequency. For example, δ_u may increase when f_e is decreased by an increase in v_e only. What this implies is, in effect, that *the unsteady boundary layer can become thicker than the steady boundary layer, particularly at high Reynolds number.*

We direct our interest to a perturbation expansion where

$$\alpha, \beta, \epsilon \ll 1. \tag{8}$$

Physically this may be visualized as follows. The amplitude of unsteady disturbances is small and, compared with the lengthscale of the cylinder radius, the *unsteady* boundary layer is thin. Within the unsteady layer an even thinner *steady* boundary layer is embedded.† Therefore, near any cylindrical surface the structure of the flow

† We assume that, for the steady and unsteady boundary layer alike, the thickness of the thermal boundary layer is of the same order as that of the momentum boundary layer, Pr being around unity.

divides radially into three layers: (*a*) the steady boundary layer adherent to the wall, (*b*) the middle layer, which stretches from the outer edge of the steady boundary layer to that of the unsteady boundary layer, and (*c*) the inviscid core outside the unsteady boundary layer.

With regard to the governing equations whose flow variables are to be expanded in power series of α, β and ϵ in order to obtain the streaming, one should, in principle, start with the full unsteady compressible Navier–Stokes equations rather than the boundary-layer equations. The reason is as follows.

As is well known, acoustic streaming stems from the temporal average of the products between the first-order quantities. Thus, if we start from the conventional boundary-layer equations, which correspond of course to the first-order approximation to the full Navier–Stokes equations, questions may arise about the effects of what is collectively called the higher-order approximation to boundary-layer theory (e.g. Van Dyke 1969) on streaming. In this connection, upon treating the problem of streaming around an oscillating cylinder, Stuart (1966) justly voiced a note of caution on the possible effect of curvature, which could be of the same second order as streaming itself. In the present case we are besieged by more than one effect of possible second-order correction. For example, both steady and unsteady boundary layers formed over the cylindrical surfaces present the problem of a steady as well as an unsteady displacement thickness; the fluctuation of temperature gives rise to changes in the viscosity which, coupled with a temporal variation in strains, might beget additional Reynolds stresses; the flow being compressible, even the effect of the second coefficient of viscosity may have to be assessed, as has in fact been done by Van Dyke (1962*a*) for steady compressible boundary layers.

To face these problems once and for all, the present author (Kurosaka 1980) abandoned the standard boundary-layer equations, and started afresh from the full compressible and unsteady Navier–Stokes equations, retaining even the second coefficient of viscosity. Under the conditions of (8), the matched asymptotic expansion in α, β and ϵ was used to ferret out the leading term of acoustic streaming, which was shown to be $O(\alpha)$; in the middle layer, the radial coordinate was scaled to δ_u; and the steady flow fields, corresponding to those outside the steady boundary layer, were expanded around the values at its outer edge, in a manner analogous to the procedure of Cole (1968, p. 16). Then, in the middle-layer equations up to the order of α, *the steady-flow properties appear as constant* evaluated at the outer edge of the steady boundary layer, rather than as the spatially changing variables, the reason being that δ_u *is much smaller than the scale of the inviscid core, the cylinder radius*. As regards the region within the steady boundary layer, whose complexity has been pointed out in §2, the difficulty was circumvented *by transferring* the boundary condition on the unsteady flow from the wall *to the innermost edge of the middle layer*; this in effect bypasses the steady boundary layer – a procedure wholly justifiable for $O(\alpha)$, not to mention $O(1)$ terms, because the ratio of the thickness of the steady boundary layer to R is $O(\epsilon\beta)$.

The consequences of the matched asymptotic expansion are as follows. As far as the terms up to $O(\alpha)$ are concerned, the governing equations in the middle layer are independent of such second-order effects as surface curvature, steady or unsteady displacement, or of the second coefficient of viscosity. (That the leading term of the streaming near the boundary remains unaffected by surface curvature and unsteady

displacement is not unexpected from the analysis of Riley (1967), who confirmed this for an incompressible stationary-flow problem). In fact, the equations are none other than those derivable from the *conventional boundary-layer equations* – where the *base steady-state variables are evaluated at the outer edge of the steady boundary layer*, those with subscript e – and they are subject to the usual wall boundary conditions.

In the light of this justification and in an effort to avoid the inevitably elaborate algebra involved in starting from the full Navier–Stokes equations, we take the following standard boundary-layer equations as those governing the flow in the middle layer:

$$\frac{\partial \rho}{\partial t}+\frac{\partial(\rho u)}{\partial n}+\frac{1}{R}\frac{\partial(\rho v)}{\partial \theta}+\frac{\partial(\rho w)}{\partial z}=0, \tag{9a}$$

$$\frac{\partial p}{\partial n}=0, \tag{9b}$$

$$\rho L_{\mathrm{m}}(v)=-\frac{1}{R}\frac{\partial p}{\partial \theta}+\frac{\partial}{\partial n}\left(\mu\frac{\partial v}{\partial n}\right), \tag{9c}$$

$$\rho L_{\mathrm{m}}(w)=-\frac{\partial p}{\partial z}+\frac{\partial}{\partial n}\left(\mu\frac{\partial w}{\partial n}\right), \tag{9d}$$

$$\rho c_p L_{\mathrm{m}}(T)-L_{\mathrm{m}}(p)=\frac{c_p}{Pr}\frac{\partial}{\partial n}\left(\mu\frac{\partial T}{\partial n}\right)+\mu\left[\left(\frac{\partial v}{\partial n}\right)^2+\left(\frac{\partial w}{\partial n}\right)^2\right], \tag{9e}$$

$$p=c_v(\gamma-1)\rho T, \tag{9f}$$

where

$$L_{\mathrm{m}}=\frac{\partial}{\partial t}+u\frac{\partial}{\partial n}+\frac{v}{R}\frac{\partial}{\partial \theta}+w\frac{\partial}{\partial z}$$

and $n=r-R$ is the boundary-layer coordinate normal to the surface.

In accordance with our preceding discussion and subject to the restrictions imposed by (8), we expand the flow variables around those steady values with subscript e, the external flow at the outer edge of the steady boundary layer, in the form

$$\left.\begin{aligned} u &= u'+u''+\ldots,\\ v &= v_{\mathrm{e}}+v'+v''+\ldots,\\ w &= w_{\mathrm{e}}+w'+w''+\ldots, \end{aligned}\right\} \tag{10}$$

and so forth, where v_{e}, w_{e}, ... are constants. The rest of the terms represents the unsteady disturbances; the single-primed terms, when divided by the amplitude of disturbances $\tilde{v}_{\mathrm{e}}$, are $O(1)$; the double-primed terms, rendered in the same form, are $O(\alpha)$; for example

$$O\left(\frac{u'}{\tilde{v}_{\mathrm{e}}}\right)=1, \quad O\left(\frac{u''}{\tilde{v}_{\mathrm{e}}}\right)=\alpha. \tag{11}$$

The temporal averages of u'', v'' and w'' give the leading terms of the acoustic streaming; as mentioned, the terms corresponding to the $O(\beta)$, $O(\epsilon)$ and other higher orders do not contribute to the leading term of the d.c. component, and are neglected in the above expansion. In accordance with our aforementioned conclusions drawn by the method of the matched asymptotic expansions, the boundary conditions for the unsteady disturbances are given, at $n=0$, as

$$\left.\begin{aligned} &u'=u''=v'=v''=w'=w''=0,\\ &T'=T''=0 \quad \text{or} \quad \frac{\partial T'}{\partial n}=\frac{\partial T''}{\partial n}=0. \end{aligned}\right\} \tag{12}$$

The flow in the inviscid core is, of course, governed by the following inviscid equations:

$$\frac{\partial \rho}{\partial t}+\frac{1}{r}\frac{\partial (r\rho u)}{\partial r}+\frac{1}{r}\frac{\partial (\rho v)}{\partial \theta}+\frac{\partial (\rho w)}{\partial z}=0, \tag{13a}$$

$$\rho\left[L_1(u)-\frac{v^2}{r}\right]=-\frac{\partial p}{\partial r}, \tag{13b}$$

$$\rho\left[L_1(v)+\frac{uv}{r}\right]=-\frac{1}{r}\frac{\partial p}{\partial \theta}, \tag{13c}$$

$$\rho L_1(w)=-\frac{\partial p}{\partial z}, \tag{13d}$$

$$L_1\left(c_p \log\frac{T}{p^{(\gamma-1)/\gamma}}\right)=0, \tag{13e}$$

$$p=c_v(\gamma-1)\rho T, \tag{13f}$$

where

$$L_1=\frac{\partial}{\partial t}+u\frac{\partial}{\partial r}+\frac{v}{r}\frac{\partial}{\partial \theta}+w\frac{\partial}{\partial z}.$$

The corresponding expansions for the flow variables in the inviscid core are given by

$$\left.\begin{aligned} u &= u'+u''+\ldots,\\ v &= v_0(r)+v'+v''+\ldots,\\ w &= w_0(r)+w'+w''+\ldots, \end{aligned}\right\} \tag{14}$$

and the like, where the orders of the primed terms are the same as those in the middle layer, (11).

4. First- and second-order problems; streaming

Substitution of the expansion series from § 3 into the corresponding governing equations yields a set of equations appropriate for each order. In this section we assemble them in hierarchic order and present solutions, together with some comments on salient features.

4.1. *First order in inviscid core*

We set

$$u'=\tilde{u}(r)\,e^{i(m\theta+kz-\omega t)},\quad v'=\tilde{v}(r)\,e^{i(m\theta+kz-\omega t)}, \tag{15}$$

and so forth, and obtain the following set of linearized equations in the inviscid core:

$$i\left(f\tilde{\rho}+\frac{1}{r}\rho_0 m\tilde{v}+\rho_0 k\tilde{w}\right)+\frac{1}{r}\frac{d}{dr}(r\rho_0\tilde{u})=0, \tag{16a}$$

$$if\tilde{u}-2\frac{v_0}{r}\tilde{v}=\frac{\tilde{\rho}}{\rho_0^2}\frac{dp_0}{dr}-\frac{1}{\rho_0}\frac{d\tilde{p}}{dr}, \tag{16b}$$

$$if\tilde{v}+\left(\frac{dv_0}{dr}+\frac{v_0}{r}\right)\tilde{u}=-\frac{im}{r\rho_0}\tilde{p}, \tag{16c}$$

$$if\tilde{w}=-\frac{ik}{\rho_0}\tilde{p}, \tag{16d}$$

$$\frac{\tilde{T}}{T_0} - \frac{\gamma - 1}{\gamma}\frac{\tilde{p}}{p_0} = 0, \tag{16e}$$

$$\tilde{p} = c_v(\gamma - 1)(\rho_0 \tilde{T} + T_0 \tilde{\rho}), \tag{16f}$$

subject to the boundary condition

$$\tilde{u}(r = R) = 0 \quad (R = r_1, r_0). \tag{16g}$$

In deriving them, use is made of (3), and w_0 is assumed to be constant.

Note that in the above the frequency ω appears solely in the form of f, defined by (4), as mentioned previously; once the profile of the steady swirl $v_0(r)$ is specified, (16*a–g*) are complete and determine ω as a function of m, k and cylinder geometry. Such a frequency–swirl relationship, obtained by both an analytical and numerical method, is presented in the appendix for the specific swirl distribution corresponding to the Rankine vortex with a single pipe.

Inspection of (16) also reveals that if $\tilde{u}$ is imaginary, the other amplitudes, $\tilde{v}$, $\tilde{w}$, $\tilde{\rho}$ etc., are real: the real parts of u' and of all the others oscillate with a phase difference equal to $\frac{1}{2}\pi$. This implies that when we proceed to the second-order terms the temporal averages of the cross-products between u' and any other flow variable must vanish.

4.2. *First order in middle layer*

We set

$$u' = \tilde{u}(n)\, e^{i(m\theta + kz - \omega t)}, \quad v' = \tilde{v}(n)\, e^{i(m\theta + kz - \omega t)}, \tag{17}$$

and so forth, and obtain the following linearized viscous equations in the middle layer:

$$i\left(f_e\tilde{\rho} + \frac{1}{R}\rho_e m\tilde{v} + \rho_e k\tilde{w}\right) + \rho_e \frac{d\tilde{u}}{dn} = 0, \tag{18a}$$

$$\tilde{p} = -\frac{R}{m}\rho_e f_e \tilde{v}_e, \tag{18b}$$

$$i\rho_e f_e \tilde{v} = i\rho_e f_e \tilde{v}_e + \mu_e \frac{d^2\tilde{v}}{dn^2}, \tag{18c}$$

$$i\rho_e f_e \tilde{w} = i\frac{kR}{m}\rho_e f_e \tilde{v}_e + \mu_e \frac{d^2\tilde{w}}{dn^2}, \tag{18d}$$

$$ic_p \rho_e f_e \tilde{T} + i\frac{\rho_e R}{m} f_e^2 \tilde{v}_e = \frac{c_p}{Pr}\mu_e \frac{d^2\tilde{T}}{dn^2}, \tag{18e}$$

$$-\frac{R}{m}\frac{\rho_e}{p_e} f_e \tilde{v}_e = \frac{\tilde{T}}{T_e} + \frac{\tilde{\rho}}{\rho_e}, \tag{18f}$$

where $\tilde{v}_e$, as mentioned, is the amplitude of v' in the inviscid core, evaluated on the cylinder surface; the boundary conditions are

$$\tilde{u} = \tilde{v} = \tilde{w} = 0, \quad \tilde{T} = 0 \quad \text{or} \quad \frac{d\tilde{T}}{dn} = 0 \quad (n = 0), \tag{18g}$$

$$\tilde{v} = \tilde{v}_e, \quad \tilde{w} = \frac{kR}{m}\tilde{v}_e, \quad \tilde{T} = -\frac{R}{c_p m} f_e \tilde{v}_e, \quad \tilde{\rho} = -\frac{R\rho_e}{m a_e^2} f_e \tilde{v}_e \quad (|n| \to \infty), \tag{18h}$$

where (18*b*) expresses the constancy of the pressure across the middle layer, and (18*h*) the matching of flow variables at its outer edge, where all are expressed in terms of $\tilde{v}_e$. $|n| \to \infty$ is to be interpreted in the usual matching sense, with the radial coordinate scaled to δ_u; $a_e^2 = c_v \gamma(\gamma-1) T_e$.

Given $\tilde{v}_e$, (18) is completely determined; the solution corresponding to a thermal condition on the wall, $\tilde{T}' = 0$, is given by

$$\tilde{u} = \tilde{v}_e \frac{im}{R} \operatorname{sgn}(n) \left\{ |n| \left[\left(\frac{Rf_e}{ma_e}\right)^2 - 1 - \left(\frac{kR}{m}\right)^2 \right] + \left[1 + \left(\frac{kR}{m}\right)^2 \right] \frac{1}{\Delta} g + \left(\frac{Rf_e}{ma_e}\right)^2 \frac{\gamma-1}{Pr^{\frac{1}{2}}\Delta} (1-h) \right\}, \tag{19a}$$

$$\tilde{v} = \tilde{v}_e g, \quad \tilde{w} = \tilde{v}_e \frac{kR}{m} g, \tag{19b, c}$$

$$\tilde{\rho} = -\tilde{v}_e \frac{R\rho_e f_e}{ma_e^2} [1 + (\gamma-1)h], \tag{19d}$$

$$\tilde{p} = -\tilde{v}_e \frac{R\rho_e}{m} f_e, \quad \tilde{T} = -\tilde{v}_e \frac{Rf_e}{c_p m} (1-h), \tag{19e, f}$$

where

$$g = 1 - \exp(-\Delta|n|), \quad h = \exp(-Pr^{\frac{1}{2}}\Delta|n|),$$

$$\operatorname{sgn}(n) = \begin{cases} 1 & (n > 0), \\ -1 & (n < 0), \end{cases}$$

$$\Delta = \sqrt{\tfrac{1}{2}}(1 \pm i) \left| \frac{f_e}{\nu_e} \right|^{\frac{1}{2}} \quad (+ \text{ sign for } f_e > 0; \quad - \text{ sign for } f_e < 0).$$

For a thermally insulated wall, the results can be obtained formally from (19) by letting $Pr \to \infty$. With regard to the fluctuating component of viscosity μ' needed for the next second-order calculation, it is related to T' by the viscosity law

$$\mu' = \left. \frac{d\mu}{dT} \right|_{T=T_e} T'. \tag{19g}$$

4.3. *Second order in middle layer*

We set

$$u'' = \overline{u''} + \mathscr{R}[A(n) e^{2i(m\theta+kz-\omega t)}], \tag{20a}$$

$$v'' = \overline{v''} + \mathscr{R}[B(n) e^{2i(m\theta+kz-\omega t)}], \tag{20b}$$

and the like, where the first terms with overbars represent the temporal averages taken over a period of oscillation $2\pi/\omega$; $\mathscr{R}$ denotes the real part. The leading terms of acoustic streaming correspond to these time averages, or d.c. components, which are functions of r only, independent of θ and z. The second terms of (20*a*, *b*) correspond to the induced second harmonics, $A(n)$ and $B(n)$ being their amplitudes.

In the corresponding governing equations we separate the d.c. components from the a.c. components, our interest being focused on the former. We first list those corresponding to the continuity, tangential and axial momentum equations and the equation of energy:

$$\rho_e \frac{\overline{du''}}{dn} + \frac{d\overline{\rho' u'}}{dn} = 0, \tag{21a}$$

$$\rho_e \frac{d\overline{u'v'}}{dn} = \frac{d}{dn}\left(\overline{\mu' \frac{\partial v'}{\partial n}} \right) + \mu_e \frac{d^2\overline{v''}}{dn^2}, \tag{21b}$$

$$\rho_e \frac{d\overline{u'w'}}{dn} = \frac{d}{dn}\left(\mu' \overline{\frac{\partial w'}{\partial n}}\right) + \mu_e \frac{d^2\overline{w''}}{dn^2}, \tag{21c}$$

$$c_p\left[\overline{\rho' \frac{\partial T'}{\partial t}} + \rho_e \overline{u' \frac{\partial T'}{\partial n}} + \frac{\rho_e}{R}\overline{v' \frac{\partial T'}{\partial \theta}} + \frac{v_e}{R}\overline{\rho' \frac{\partial T'}{\partial \theta}} + \rho_e \overline{w' \frac{\partial T'}{\partial z}} + w_e \overline{\rho' \frac{\partial T'}{\partial z}}\right]$$
$$- \left[\frac{1}{R}\overline{v' \frac{\partial p'}{\partial \theta}} + \overline{w' \frac{\partial p'}{\partial z}}\right]$$
$$= \frac{c_p}{Pr}\frac{d}{dn}\left(\mu' \overline{\frac{\partial T'}{\partial n}}\right) + \frac{c_p}{Pr}\mu_e \frac{d^2\overline{T''}}{dn^2} + \mu_e\left[\left(\overline{\frac{\partial v'}{\partial n}}\right) + \left(\overline{\frac{\partial w'}{\partial n}}\right)^2\right]. \tag{21d}$$

The boundary conditions are as follows:

$$\overline{u''} = \overline{v''} = \overline{w''} = 0, \quad \overline{T''} = 0 \quad \text{or} \quad \frac{d\overline{T''}}{dn} = 0 \quad (n = 0), \tag{21e}$$

$$\lim_{|n|\to\infty} \frac{d\overline{v''}}{dn} = \lim_{|n|\to\infty} \frac{d\overline{w''}}{dn} = \lim_{|n|\to\infty} \frac{d\overline{T''}}{dn} = 0 \quad (n \to \infty). \tag{21f}$$

As for the boundary condition for $|n| \to \infty$, the original matching condition for $\overline{v''}$ reads

$$\overline{v''_{\mathrm{ml}}}(|n| \to \infty) = \overline{v''_{\mathrm{ic}}}(r = R),$$

where ml stands for the middle layer, ic for the inviscid core. The determination of streaming in the core will need this relationship; for the present middle layer, as in the usual case (Riley 1967; Batchelor 1967, p. 360), a weaker condition suffices: $\overline{v''_{\mathrm{ml}}}(|n| \to \infty)$ is finite, or equivalently the above $d\overline{v''}/dn \to 0$. Similar conditions apply to $\overline{w''}$ and $\overline{T''}$; one does not need conditions for $\overline{u''}$ at $|n| \to \infty$.

From (21), $\overline{u''}$, $\overline{v''}$, $\overline{w''}$ and $\overline{T''}$ are completely and uniquely determined in the middle layer. These d.c. components of velocity and temperature are dependent upon only the first-order terms in the middle layer, and independent of the streaming in the inviscid core; on the contrary, the latter will be dependent upon the former, regardless of the magnitude of the streaming Reynolds number R_s.

The solution of (21*b*) yields $\overline{v''}$. Corresponding to the thermal boundary condition where the fluctuation of temperature on the wall is maintained to be zero, the tangential streaming at the outer edge of the middle layer is given by

$$\overline{v''}(|n| \to \infty) = -\frac{m\tilde{v}_c^2}{2Rf_e}\left\{\frac{3}{2}\left[1 + \left(\frac{kR}{m}\right)^2\right] - G + (\gamma - 1)\frac{G}{Pr(Pr+1)}\right.$$
$$\left. - G(\gamma - 1)\frac{Pr}{Pr+1}\left(\frac{3}{2} - \frac{T_e}{T_e + T_1}\right)\right\}, \tag{22a}$$

where

$$G = (Rf_e/ma_e)^2. \tag{22b}$$

This we regard as one of our central results of analysis.

In obtaining this, an explicit relationship between viscosity and temperature appearing in (19*g*) is needed, and for this we have chosen Sutherland's formula

$$\mu = \mu^*\left(\frac{T}{T^*}\right)^{\frac{3}{2}}\frac{T^* + T_1}{T + T_1},$$

when μ^* is the viscosity at the reference temperature T^* and T_1 is, for air, 114 K.

Once the frequency–swirl relationship – obtainable from the linearized equation in the inviscid core for a specified swirl distribution – is substituted in f_e appearing

in the above and defined by (5b), streaming is completely determined; we note that $\overline{v''}/\tilde{v}_e$ is $O(\alpha)$.

The axial streaming is related to the tangential streaming by

$$\overline{w''}(|n| \to \infty) = \frac{kR}{m}\overline{v''}(|n| \to \infty). \tag{23}$$

The streaming in the tangential and axial directions alike is independent of the actual value of viscosity, as expected. For our purposes we need not correct for the Stokes drift. We also emphasize that the expressions, as they stand, are not restricted to any specific radial profile of the steady flow field.

The radial streaming is given as

$$\overline{u''}(|n| \to \infty) = \pm \frac{\nu_e^{\frac{1}{2}}|f_e|^{\frac{1}{2}}}{2\sqrt{2}\,a_e^2}\tilde{v}_e^2\left\{1+\left(\frac{kR}{m}\right)^2+\left(\frac{Rf_e}{ma_e}\right)^2\frac{\gamma-1}{Pr^{\frac{1}{2}}}\right\}, \tag{24}$$

where + corresponds to the streaming near the surface $r = r_i$ and − to $r = r_o$; the radial streaming is now dependent upon the viscosity.

For a thermally insulated wall, the results can be obtained formally from the above by letting $Pr \to \infty$: for example, the tangential streaming becomes

$$\overline{v''}(|n| \to \infty) = -\frac{m\tilde{v}_e^2}{2Rf_e}\left\{\frac{3}{2}\left[1+\left(\frac{kR}{m}\right)^2\right]-G-G(\gamma-1)\left(\frac{3}{2}-\frac{T_e}{T_e+T_1}\right)\right\}, \tag{25}$$

and the like.

We now pause and confirm that the expressions (22) or (25) for the tangential streaming embrace the well-known results as their special cases. In the present representation of disturbances $e^{i(m\theta+kz-\omega t)}$, let $k = 0$, and in the place of θ introduce the circumferential distance x measured along the perimeter of the cylinder. Thus the disturbance may be regarded as a plane wave travelling in the x-direction: $e^{i(lx-\omega t)}$, where $l = m/R$. Furthermore, we restrict our attention to a fluid otherwise in a state of rest: $v_e = w_e = 0$. If the fluid is incompressible, G vanishes in the limit of $a_e \to \infty$ and (22) or (25) becomes

$$\overline{v''}(|n| \to \infty) = \frac{3}{4}\frac{l\tilde{v}_e^2}{\omega}. \tag{26}$$

This is but a classical result of streaming at the outer edge of the unsteady shear layer (e.g. Batchelor 1967, p. 360).

On the other hand, if the fluid is compressible, G is easily shown to be unity, and (25), corresponding to a thermally insulated wall, is reduced to

$$\overline{v''}(|n| \to \infty) = \frac{l\tilde{v}_e^2}{4\omega}\left\{1-(\gamma-1)\left(3-\frac{2T_e}{T_e+T_1}\right)\right\}. \tag{27}$$

The second term in the curly bracket corresponds to the streaming induced by the Reynolds stress that is caused by the variation of the viscosity due to the temperature fluctuation, the first term on the right-hand side of (21b). Numerically, this is by no means small; for instance, at $T_e = 20$ °C = 293 K, the second term of (27) is equal to 0·62, compared with unity of the first term. This notwithstanding, if we choose to ignore it, (27) becomes

$$\overline{v''}(|n| \to \infty) = \frac{l\tilde{v}_e^2}{4\omega}, \tag{28}$$

which is equal to $\tilde{v}_e^2/4a_e$, also a classical result for compressible flow (e.g. Lighthill 1978b, p. 347).

Compare (28), the streaming induced by a one-dimensional wave in the absence of base flow, with our general result (22) or (25) for the cylindrical waves where the base steady flow is present. We note that the factors outside the curly bracket of (22) or (25) can immediately be obtained from (28) by replacing l by m/R, and ω by f_e. The former corresponds, as noted, to the curvature effect. The latter is the Doppler effect apparent to an observer situated on the frame of reference in helical motion, advancing axially with w_e, while rotating with v_e.

This much settled, we now turn to the radial momentum equation and the equation of state, related to the temporal averages of the pressure $\overline{p''}$ and density $\overline{\rho''}$. In contrast to the d.c. components of velocity and temperature, they cannot be determined from the following corresponding equations of the middle layer alone:

$$d\overline{p''}/dn = 0, \tag{29a}$$

$$\overline{p''} = c_v(\gamma-1)\,(\rho_e\overline{T''}+\overline{\rho'T'}+T_e\overline{\rho''}). \tag{29b}$$

If we were to solve them, $\overline{p''}$ and $\overline{\rho''}$ would have to be matched, at the outer edge of the middle layer, with the corresponding quantities in the inviscid core.

4.4. *Second order inviscid core*

Even in the core, we write the second-order disturbances in the form of (20); there, the temporal average term is still the leading term of the streaming in the core. Between the streaming in the middle layer and the inviscid core, the difference is that the latter is now driven by the former. This remains so regardless of the value of the streaming Reynolds number R_s, no matter how large or small (here R_s is defined as $R_s = (\alpha/\beta)^2$). However, as is now well known, the structure of the streaming outside the unsteady boundary layer is strongly dependent upon R_s, as first pointed out by Stuart (1963, p. 384).

If we take simply the temporal average of the second-order equations in the core, they, of course, correspond to the case of $R_s \ll 1$, and are given by

$$\overline{u''} = 0, \tag{30a}$$

$$-2\rho_0 v_0\frac{\overline{v''}}{r}-\frac{v_0^2}{r}\overline{\rho''}+\frac{1}{r}\frac{\partial}{\partial r}(r\rho_0\overline{u'^2})-\frac{1}{r}\rho_0\overline{v'^2}-2\frac{v_0}{r}\overline{\rho'v'} = -\frac{\partial\overline{p''}}{\partial r}, \tag{30b}$$

$$\overline{p''} = c_v(\gamma-1)\,(\rho_0\overline{T''}+\overline{\rho'T'}+T_0\overline{\rho''}), \tag{30c}$$

with the boundary conditions $\overline{u''} = 0$ on the walls, and

$$\overline{v''_{ic}}(r=R) = \overline{v''_{ml}}(|n|\to\infty), \tag{30d}$$

$$\overline{w''_{ic}}(r=R) = \overline{w''_{ml}}(|n|\to\infty), \tag{30e}$$

$$\overline{T''_{ic}}(r=R) = \overline{T''_{ml}}(|n|\to\infty), \tag{30f}$$

with similar matching conditions for $\overline{p''}$ and $\overline{\rho''}$, as stated at the end of §4.3. In deriving them, we have taken due account of the phase relationship between u' and others, stated in §4.1. Missing from the above set is the energy equation which, once time-averaged, vanishes identically. The equation of continuity and the momentum equations in θ- and z-directions all collapse to yield (30*a*).

Since viscous terms are absent in (30*a*, *b*) the equations are of inviscid type. Equations (30*d*, *e*) correspond, however, to the boundary conditions on the 'moving

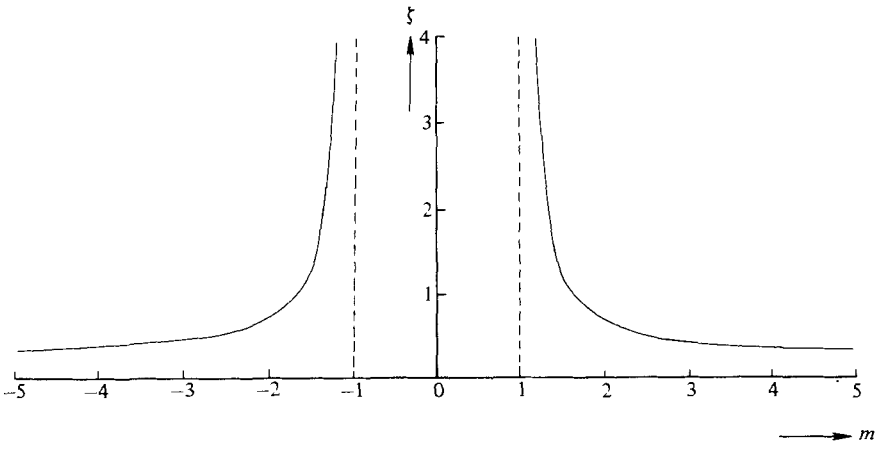

FIGURE 2. Tangential streaming near the tube periphery of a single pipe; $\lambda = 2, \kappa = 0$.

wall'; the fluid in the inviscid core is set in spiralling motion by the streaming in the middle layer. Equation (30*f*) corresponds to the prescribed surface temperature. In (30*a–c*), not only is the set of equations incomplete, but their depressed order ostensibly prevents them from satisfying the boundary conditions. However, this is in no way an indication of any kind of breakdown; the missing equations are to be supplied from the terms of *higher order* than the present second order. That this is so can best be illustrated by referring to the streaming induced by fluctuations in incompressible flow which is otherwise at rest. For $v_0 = 0$, we note that $\overline{v''}$ or the tangential velocity is now completely lost from (30*b*) or, for that matter, from everywhere else. It can be recovered only from the consideration of higher-order terms; in the terminology of the aforementioned matched asymptotic expansion of the present author, out of the viscous terms in the higher-order equations corresponding to $\tilde{v}_e O(\alpha\beta^2)$, we obtain

$$\nabla^4\overline{\Psi''} = 0, \quad \text{where} \quad \bar{v}'' = \frac{\partial\overline{\Psi''}}{\partial r},$$

which is the biharmonic equation originally due to Rayleigh (1884, p. 244) and derived anew by Riley (1967) using matched asymptotic expansions.

The foregoing discussion illustrates the fact that higher-order series terms in an expansion scheme are needed, in general, to determine the leading term of streaming in the core; this presents the entanglement of a formidable backward linking between terms in the series, as opposed to more direct forward linking.

We now turn to the case of $R_s \gg 1$. For incompressible fluid in the absence of base steady flow, the fundamental equation governing the exterior streaming was established by Riley (1967); it corresponds to the full steady Navier–Stokes equation, where R_s replaces the Reynolds number; thus, in order to solve this problem, nothing short of numerical computations (Duck & Smith 1979; Haddon & Riley 1979) seems to be effective. In the present situation of a compressible fluid where the base steady flow exists, there appears no reason to expect that the governing equation would become simpler.

In the face of these complications, we shall make no attempt to derive streaming in the core, being content instead that the phenomena of interest can be explained,

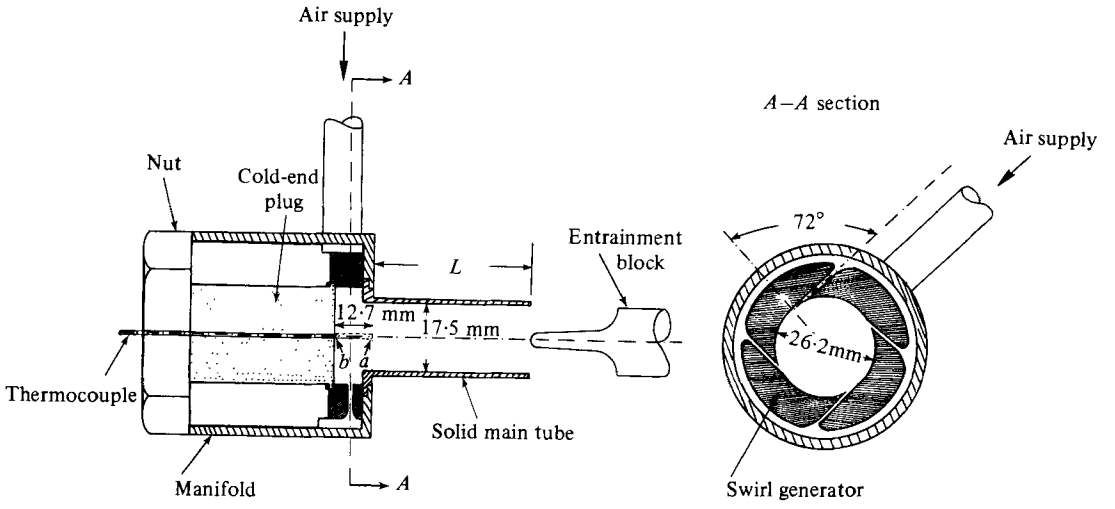

FIGURE 3. Layout of baseline configuration; solid main tube.

as seen shortly, by inspecting the change in behaviour of the streaming at the outer edge of the middle layer, whose lead the streaming in the core follows.

5. Application to Ranque–Hilsch tube

5.1. *Frequency and results of streaming analysis*

As a model 'inviscid' steady velocity profile corresponding to a Ranque–Hilsch tube of uniflow type, we consider a Rankine vortex within a single tube represented by

$$v_0(r) = \Omega r \quad (0 < r < r^*), \tag{31a}$$

$$v_0(r) = \Gamma/r \quad (r^* < r < r_0), \tag{31b}$$

where $\Gamma = \Omega r^{*2}$, and r^* denotes the radius at the interface between a forced and free vortex. We are interested in the unsteady disturbance with $k \to 0$ and the first radial mode.

As shown in the appendix, the frequency–swirl relationship for such a case, determined from linearized equations in the inviscid core, can be represented adequately by

$$\omega = \pm (|m| - 1 + \lambda^{-2|m|}) \frac{\Gamma}{r^{*2}}, \tag{32}$$

$\pm$ sign corresponding to $m > 0$ or $m < 0$ respectively. Although the relationship is derived by neglecting the second-order terms in the swirl, even at a swirl Mach number near unity, this analytical expression still compares favourably with the numerical results of Sozou & Swithenbank (1969) (see appendix). The linear dependence of the frequency on the swirl is a singularly distinguishing feature of the vortex whistle in a single pipe discovered first by Vonnegut (1954); see also Chanaud (1963, 1965).

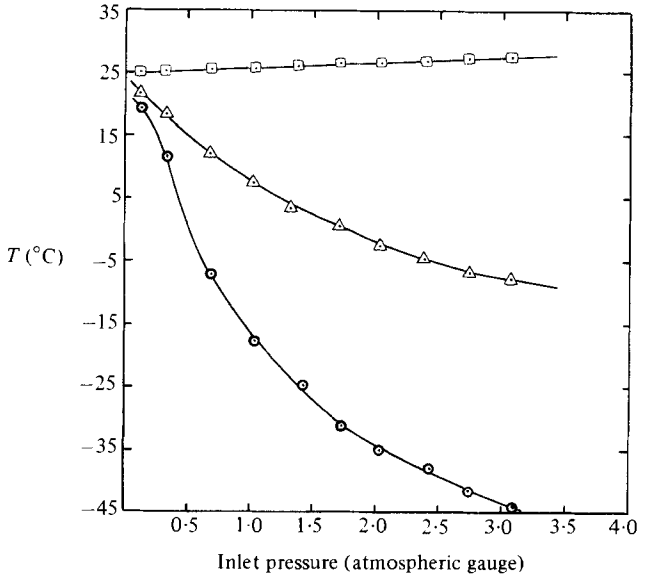

FIGURE 4. Temperature measurement for solid main tube; L = 4·19 cm: ⊡, inlet temperature; △, centreline temperature at position b of figure 3; ⊙, centreline temperature at position a of figure 3.

Substituting (32) into (22) or (25) and neglecting the second-order terms in the swirl, we obtain the streaming near the tube periphery:

$$\overline{v''}(|n| \to \infty) = \frac{\tilde{v}_e^2 \zeta}{\Gamma/r_0}, \tag{33a}$$

where

$$\zeta = \frac{3}{4} \frac{|m|}{(|m| - 1 + \lambda^{-2|m|})\lambda^2 - |m|} \tag{33b}$$

and $\lambda = r_0/r^*$. This holds regardless of the thermal conditions, adopted in deriving (22) or (25), on the tube wall.

The above equation (33) shows that the streaming remains obviously the same even when m is replaced by $-m$, and furthermore it can readily be shown that its sign is always positive:

$$\overline{v''}(|n| \to \infty) > 0,$$

no matter what the values of λ and m may be. Positive values imply that the tangential streaming is in the same direction as the steady swirl; this in turn implies that streaming near the tube periphery augments the steady swirl. The magnitude of such streaming increases as the circumferential wavenumber m decreases. Figure 2 illustrates this, where ζ of (33b) is drawn as a continuous function of the circumferential wavenumber (though in reality, of course, it takes only integer values); λ is taken to be 2. Observe the increase of ζ as m is decreased; at $m = 1$, ζ grows infinitely large, whatever λ may be, as is easily seen from (33).

This added tangential velocity near the tube periphery converts the original Rankine vortex into a forced-vortex type. Even disregarding momentarily the effect of the static temperature gradient, this metamorphosis towards a forced vortex on its own tends to separate the total temperature: the colder stream near the centre and

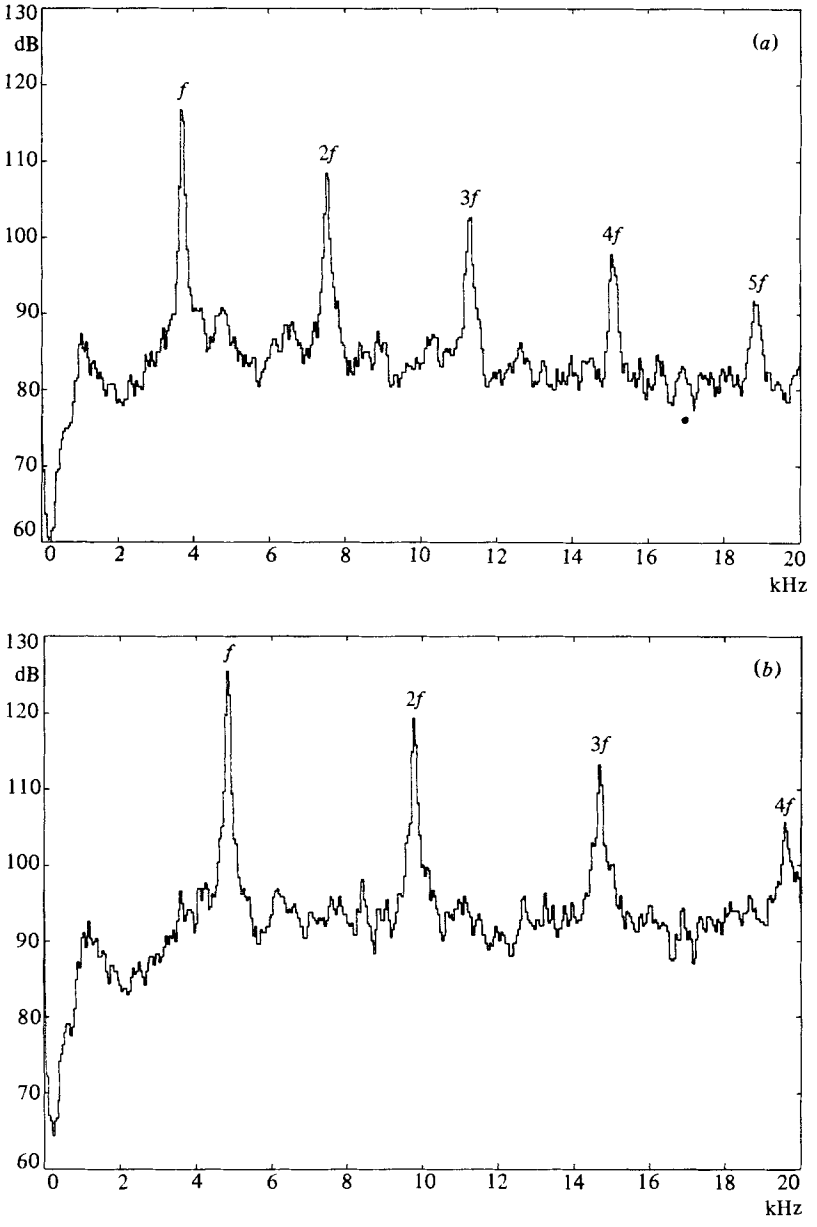

FIGURE 5. Frequency spectra for solid main tube; L = 4·19 cm: (*a*) inlet pressure = 1·02 (atmospheric gauge); (*b*) inlet pressure = 2·04 (atmospheric gauge).

the hotter stream near the periphery of the tube. This is precisely the onset of the Ranque–Hilsch effect.

As for the static temperature distribution, which in the inviscid core is determined by the total swirl, the static temperature for a forced vortex with sufficiently higher speed close to the periphery is lower than that of the Rankine vortex, provided that the temperature near the tube wall remains the same. This difference in static temperature further separates the total temperature.

Obviously, our analysis aims only at the onset of total-temperature separation. We

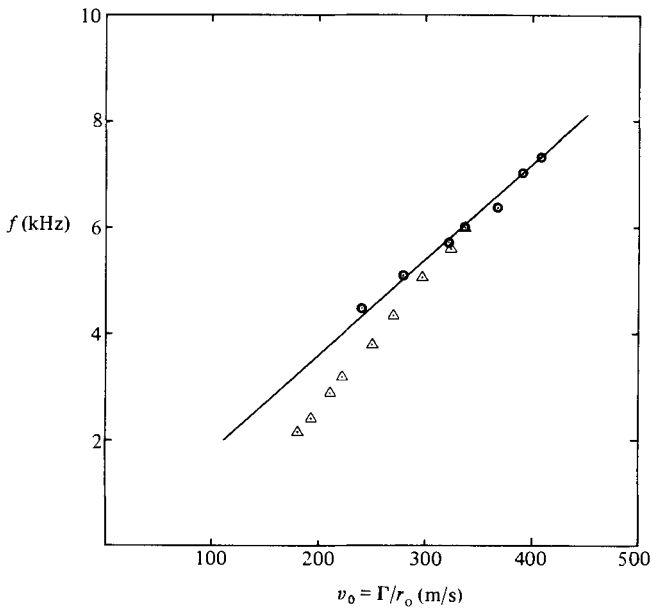

FIGURE 6. Fundamental frequency for solid main tube: ——, calculated; △, L = 4·19 cm; ⊙, L = 1·27 cm.

rest content to exhibit the initial conversion of swirl distribution, based upon the acoustic streaming, to a forced-vortex type and give no detailed calculation of the final equilibrium flow field.

Equation (33) further asserts that such a conversion of swirl should take place *regardless of the speed of the swirl*,† and regardless of the axial position within the tube, *even near its inlet*. This appears to fit in well with the previous observations: detailed measurements in the Ranque–Hilsch tube indeed show that a forced vortex is always found at any speed of swirl, and is formed immediately near the entrance to the tube even at a location as close as practically possible to the inlet nozzle (Hartnett & Eckert 1957; Scheller & Brown 1957; Lay 1959; Savino & Ragsdale 1961; Sibulkin 1962; Takahama 1965; Bruun 1969). The forced vortex occupies almost the entire cross-section, except of course for the neighbourhood of the boundary layer on the tube periphery. The radial separation of total temperature right at the tube entry, induced by the formation of the forced vortex, is also found by many experimenters. Contrast this with the ill-founded hypothesis of a gradual deterioration of a free vortex to a forced vortex in the direction of flow, which, although advocated as a mechanism of total temperature by Hilsch (1947) and Knoernschild (1948), has never been observed.

As stated, ζ becomes infinitely larger at $m = 1$, and obviously the analysis formally breaks down here. Despite this, we may expect that the trend of large streaming and the resulting total-temperature separation are indicative of what actually happens in a real flow. This we anticipate in analogy with the other similar resonance-like

† Although the presence of the steady swirl in the denominator might convey the false impression that, as the swirl increases, the amount of streaming and hence the separation of the total temperature becomes less, what actually happens is that the amplitude of the disturbance $\tilde{v}_e$ grows faster, resulting in the net increase in $\overline{v''}$.

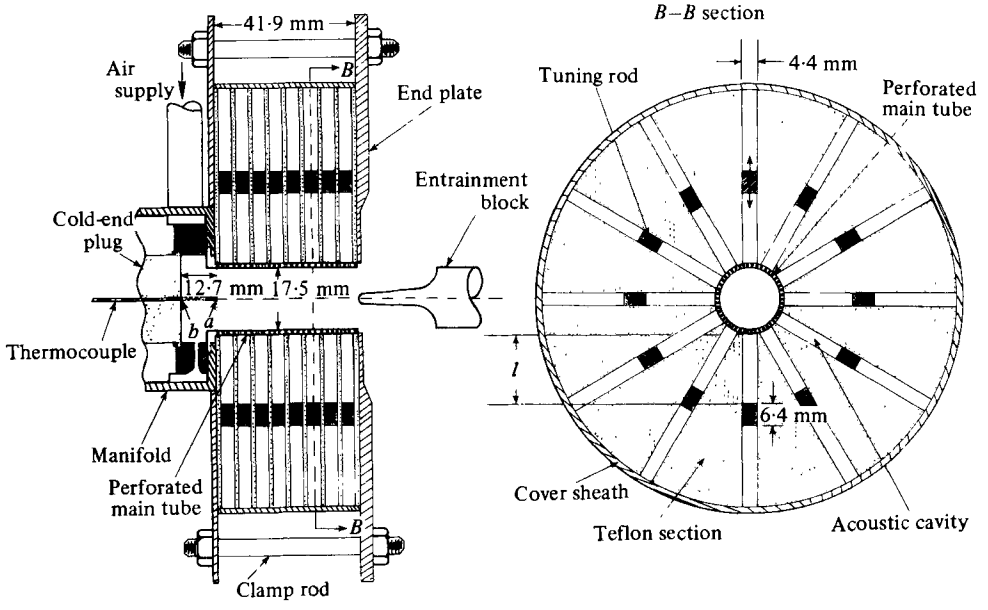

FIGURE 7. Layout of modified test rig; perforated main tube with acoustic suppressors.

phenomena; in the spirit of the present investigation, we make no attempt to expend any elaborate computational effort on this, and instead we proceed to verify this directly by experiments described next.

5.2. *Experiments*

As a prototype of the test rig, a commercially available Ranque–Hilsch tube (Vortec Corporation, model no. 328–50) was acquired: in its original form a main pipe of 22·9 cm length and 1·75 cm diameter was connected to a manifold section, where a swirl generator, with four tangentially drilled slots inclined 72° from the radial direction, was housed. Pressurized air entered the manifold and separated into two counter-flows: the open end of the main pipe, where a flow-controlling globe valve was placed, served as the exhaust for the hotter air, while the colder air discharged from an opening placed at the other end of the manifold.

5.2.1. *Baseline configuration and measurements.* Subsequently, two modifications were added to the prototype. First, the cold end in the manifold was completely closed up by a Teflon plug; the air discharged only from the main pipe. This change to a uniflow arrangement was made to ease a direct comparison with the analytical model. Secondly, on the basis of the previous discussion, where we stated that the main pipe need not be long to create the total-temperature separation, the initial tube of $L = 22{\cdot}9$ cm was replaced with a shorter brass tube of 4·19 cm. Figure 3 shows the entire layout of this uniflow test rig, which served as our baseline configuration.

With the length of the main pipe thus shortened, it was found that the use of the original globe valve at the end of the main pipe seriously affected the intensity of the pure-tone noise. Since the rig was eventually to be further modified so as to reduce the pure tone by the installation of acoustic suppressors, it was necessary to minimize such an acoustic interference in this baseline configuration. At the same time, however, a provision of some form of block at the end of the main pipe was required to prevent

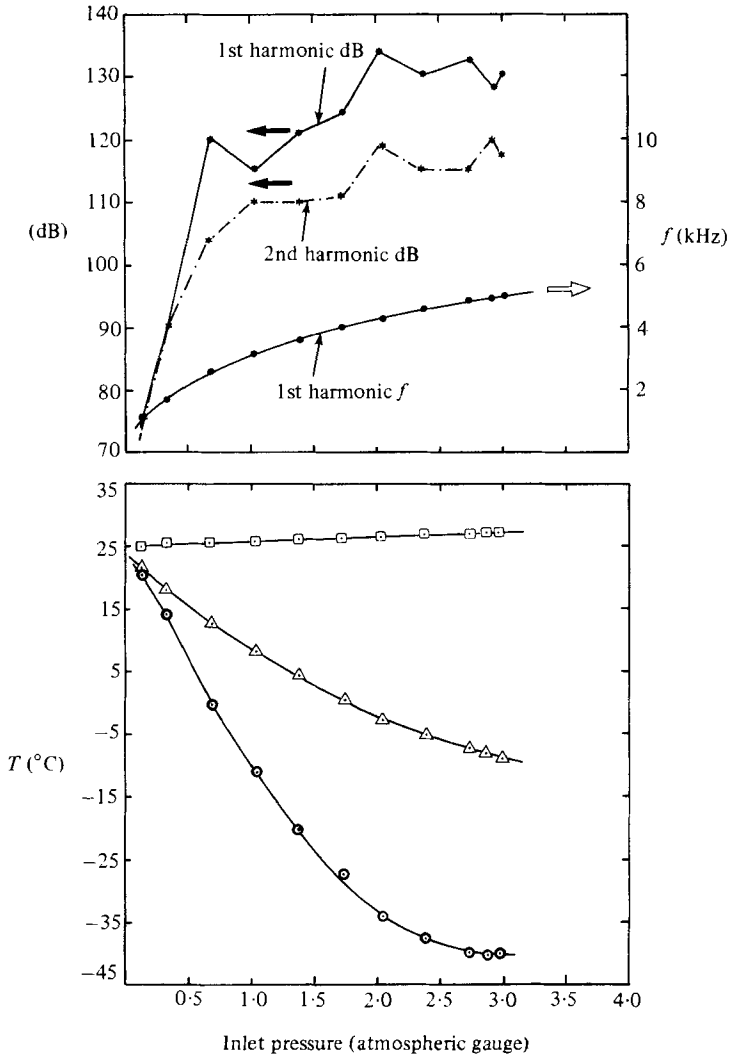

FIGURE 8. Temperature and acoustic measurement for perforated main tube with acoustic suppressors; l = 0 mm; ⊡, inlet temperature; △, centreline temperature at position b of figure 7; ⊙, centreline temperature at position a of figure 7.

the entrainment of the ambient air into the test section, which would otherwise have occurred owing to the lowered pressure at the core of the vortex. To meet these conflicting requirements, several conical shapes with different geometry were tried; among them the one with a contour shown in figure 3 was selected to block the entrainment. Unless otherwise stated, the tip of the block was always placed in the exit plane of the main pipe.

The pressurized air supplied from a separately located high-pressure tank entered the manifold via a pressure regulator, a flow-metering orifice and a sound muffler. The entire test assembly was housed inside a reverberation chamber.

A shielded type Chromel–Alumel thermocouple of 1·6 mm diameter (Omega SCASS-062G-6) was inserted through the cold-end plug. By moving it in the axial

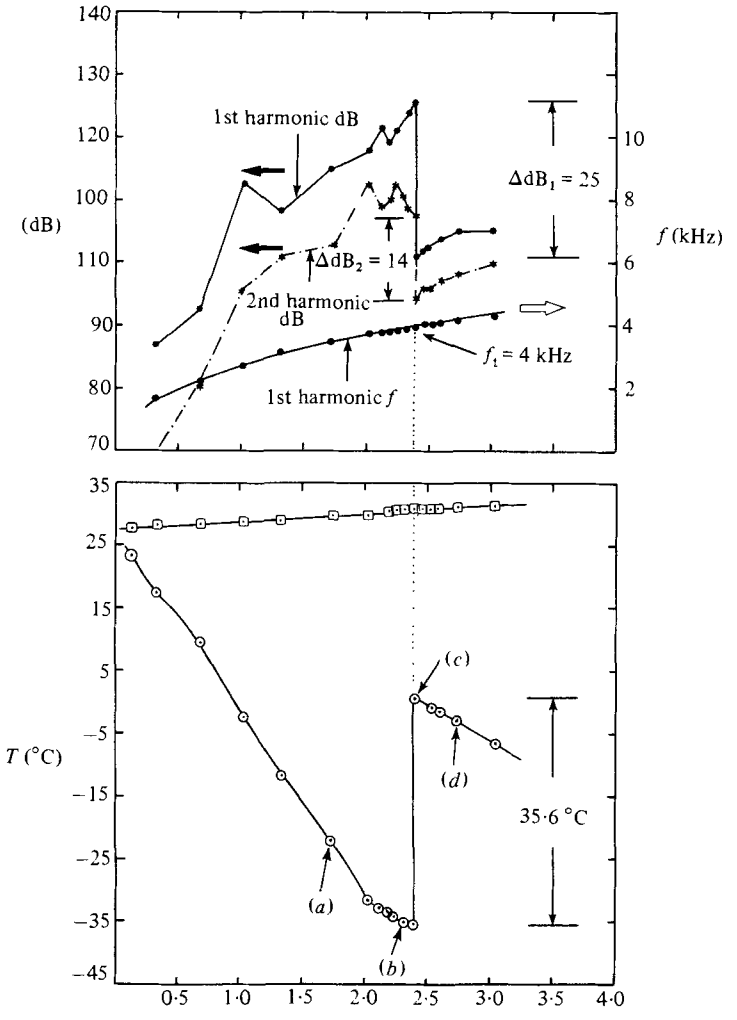

FIGURE 9. Temperature and acoustic measurement for perforated main tube with acoustic suppressors; l = 1·02 cm: ⊡, inlet temperature; ⊙, centreline temperature at position *a* of figure 7. (*a*), (*b*), (*c*) and (*d*) correspond to those of figure 10.

direction, the temperature at the centreline of the tube was traversed (see figure 3). A condenser microphone of 6·4 mm diameter (Bruel & Kjaer Type 4135), mounted nominally 91 cm away in the exit plane of the main pipe, monitored the sound; its output was fed into an FFT high-resolution signal analyser (Bruel & Kjaer Type 2033).

Figure 4 presents the dependence of the cold temperature at the centreline, together with the record of the inlet temperature. Two cold-temperature measurements are shown: one at the position where the thermocouple was flush with the cold-end plug (position *b* of figure 3) and the other at 12·7 mm away from it (position *a*). The latter corresponded to the coldest spot along the centreline. Observe that it went down as low as −45 °C. The presence of the coldest spot near the entrance to the main pipe agrees with the findings of others, referred to in §5.1; as stated,

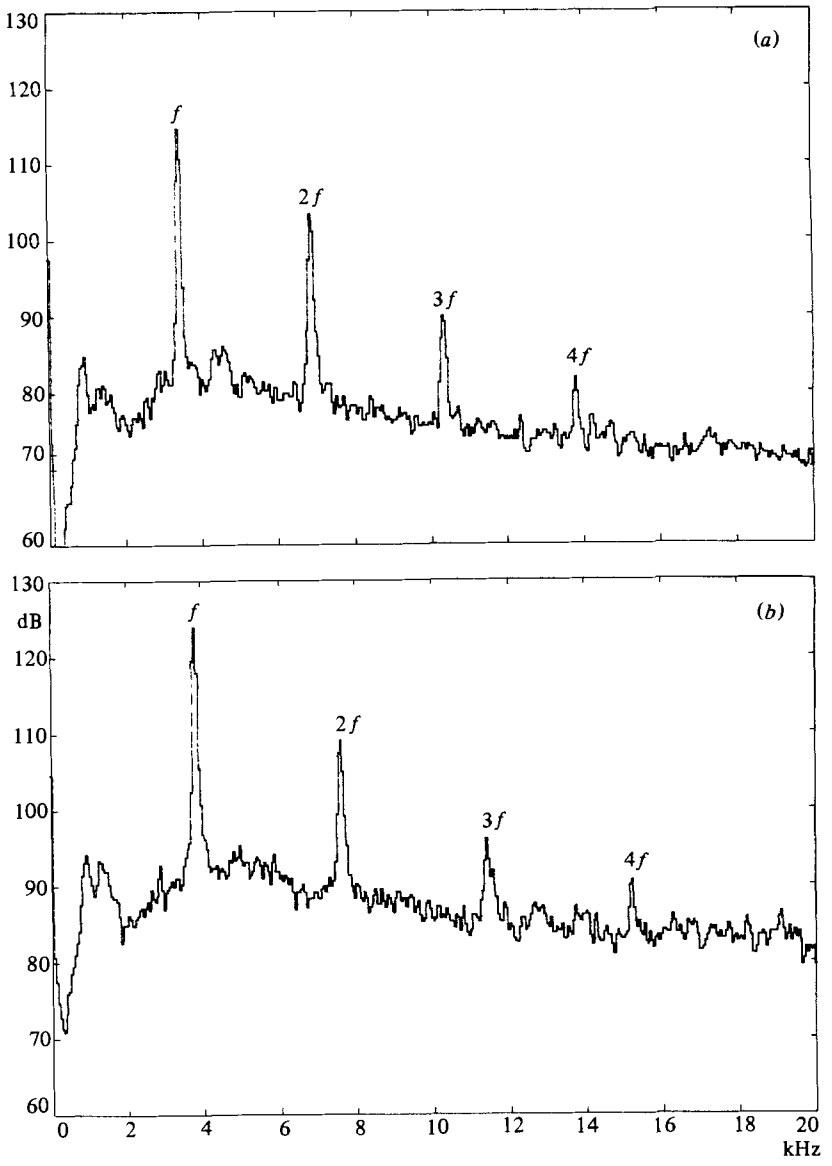

FIGURE 10 (*a*, *b*). For caption see facing page.

if the acoustic streaming is indeed a mechanism, it should cause the total-temperature separation even near the tube entrance. Note also in figure 4 that, as predicted, the temperature separation occurred even at low inlet pressure.

Figure 5 exemplifies the narrow-band frequency spectra, where we immediately recognize the predominant peaks of the first harmonic, with frequency $f = \omega/2\pi$ and its higher harmonics. The pure tones indeed overshadow the background noise, as postulated in § 1 and the analysis above. The two spectra of figure 5 at different inlet pressures illustrate, by comparison, the point that f increases as the inlet pressure is raised; note also the increase of the sound level at higher inlet pressure. A complete removal of the entrainment block from the main-pipe exhaust did not change f.

The tangential wavenumber m of the pure tones was determined by placing two

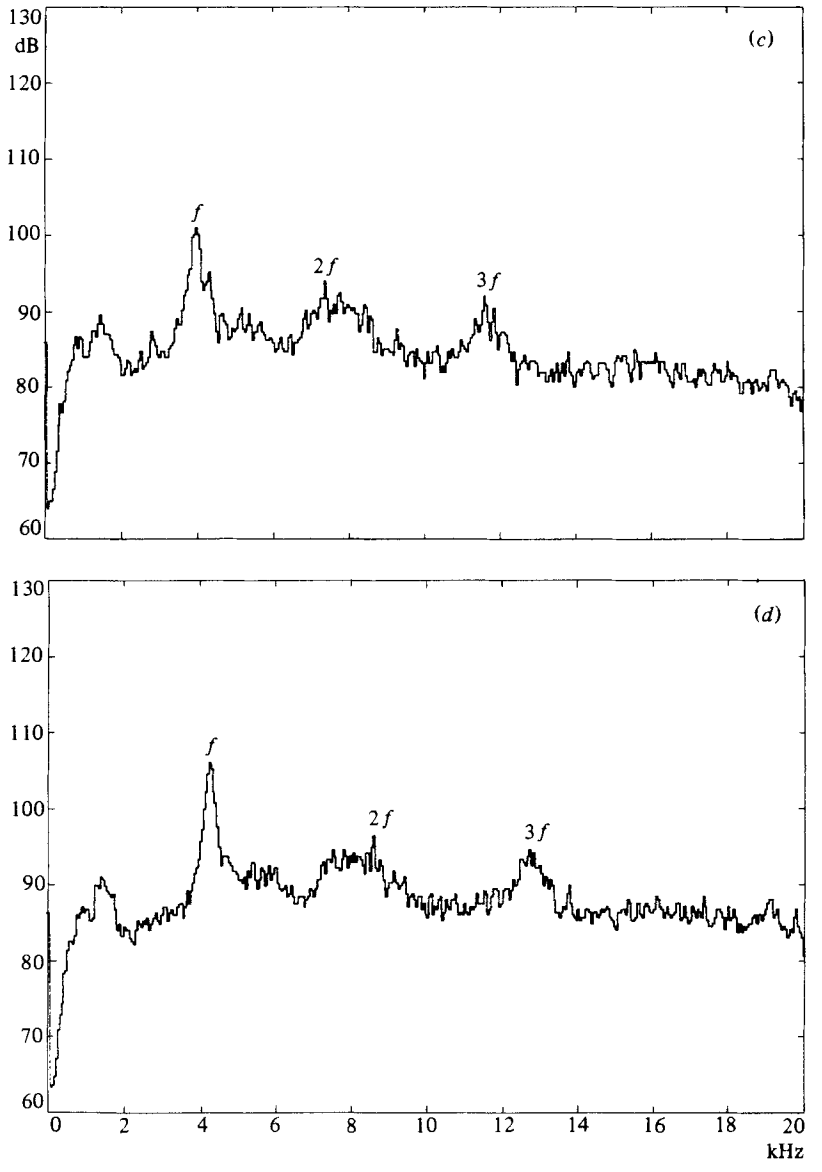

FIGURE 10. Frequency spectra for perforated main tube with acoustic suppressors; l = 1·02 cm: (*a*) inlet pressure = 1·70 (atmospheric gauge), (*b*) 2·31, (*c*) 2·38, (*d*) 2·72.

microphones at different circumferential positions around the exhaust and in the exit plane of the main pipe and by measuring their phase difference ψ in the following ways: (i) observation of Lissajous figures displayed on a dual-beam oscilloscope, and (ii) direct measurement of ψ by a phase meter (Wavetek Model 750). By filtering only the signal corresponding to the fundamental frequency f, from two microphones placed 180° apart, ψ was found to be 180°; when they were 90° apart ψ = 90°. This means m = 1 for f; the pure tone with f corresponds to the first tangential mode of a spinning wave or the vortex whistle. The result is consistent with the measurements of Chanaud (1963) made for Vonnegut's 'vortex whistle'.

As for the second harmonic, by changing the filter frequency to $2f$, from two

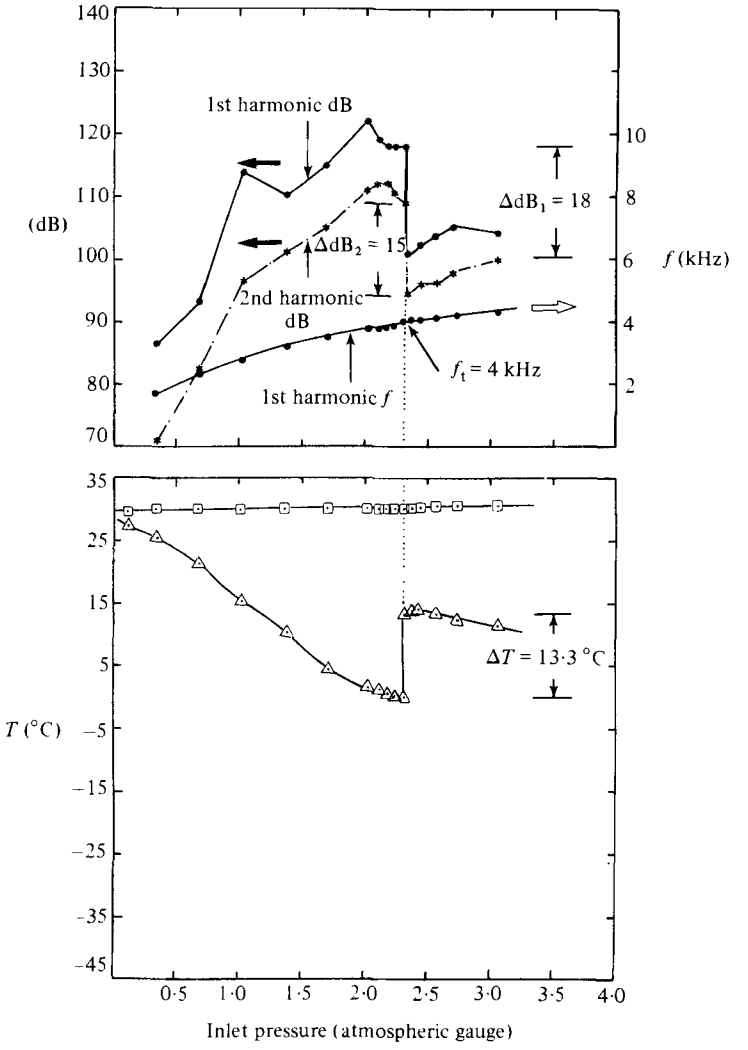

FIGURE 11. Temperature and acoustic measurements for perforated main tube with acoustic suppressors; l = 1·02 cm: □, inlet temperature; △, centreline temperature at position b of figure 7.

microphones placed 90° apart, ψ was found to be 180°; for 45° apart $\psi = 90°$. Thus the wavenumber for $2f$ is $m = 2$. The doubling of the wavenumber when the frequency is doubled corresponds unmistakably to the induced harmonics as exemplified by the second terms of (20a, b), whose form is applicable to the inviscid core as well; this attests to the presence of the second-order disturbances, as expected from analysis. The wavenumbers of the third and fourth harmonics were identified, in a similar manner, to be equal to $m = 3$ and 4 respectively.

Concerning the first harmonic or the vortex whistle, by setting $m = 1$ (32) reduces to

$$f = \frac{\omega}{2\pi} = \frac{1}{2\pi}\frac{\Gamma}{r_0^2}. \tag{34}$$

This special formula appears to have first been obtained by Sozou & Swithenbank

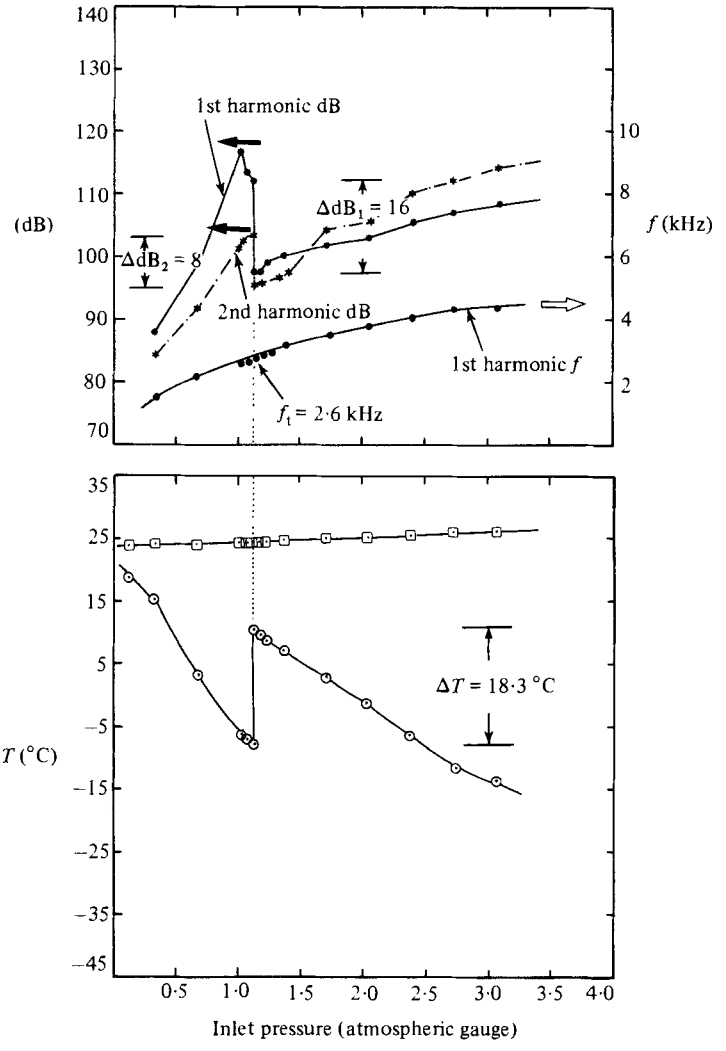

FIGURE 12. Temperature and acoustic measurement for perforated main tube with acoustic suppressors; $l = 1{\cdot}52$ cm: ⊡, inlet temperature; ⊙, centreline temperature at position a of figure 7.

(1969), who apparently found it from inspection of their numerically computed results; see their figure 8(a). Given circulation Γ and the radius of the pipe r_0, we can predict from (34) the frequency† – fortuitously even without measuring r^*, the radius of the interface in a Rankine vortex. Γ may be estimated by assuming that its value around the tube periphery is equal to that around the circumference at the exit of the swirl generator. (Given the injection angle and injection-hole area, the tangential

† Although the formula is derived for a Rankine vortex, it is also applicable to an actual forced vortex, which, on the evidence of the aforementioned measurements by previous investigators, is certainly formed within the present tube. The reason is that, because of the presence of the boundary layer near the tube periphery, any existent forced vortex is in effect a Rankine vortex with an enlarged region of a forced-vortex zone.

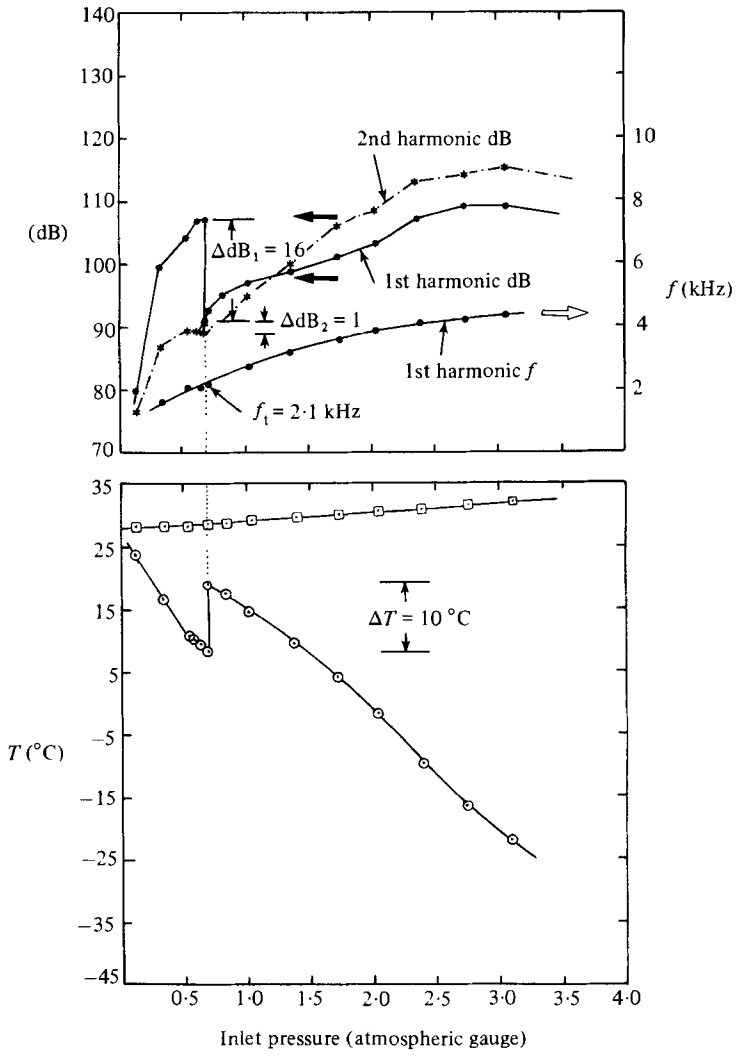

FIGURE 13. Temperature and acoustic measurement for perforated main tube with acoustic suppressors; l = 2·03 cm: ⊡, inlet temperature; ⊙, centreline temperature at position a of figure 7.

velocity is estimated by the volume flow determined from the mass flow and a static pressure tap installed on the cold-end plug.) The frequency f thus calculated is shown in figure 6, together with the measured value corresponding to the tube length of 4·19 cm. Although the agreement may not be unreasonable, the obvious discrepancy is noticeable, and it was felt that this might be due to the slowdown of swirl through the pipe. Therefore a shorter version of the main tube L = 1·27 cm was constructed and tested; although the frequency peaks were not as distinct as that for 4·19 cm, they were still well defined. The measured first harmonic, presented also in figure 6, now shows an excellent agreement with theory.

5.2.2. *Perforated main tube with acoustic suppressors.* Upon the completion of the baseline tests, the main tube of smooth brass was replaced with a perforated tube of the same diameter and length (figure 7); the tube was encased in an intermediate

Teflon section, where acoustic cavities of 4·4 mm diameter, 8 in the axial and 12 in the circumferential direction, were drilled out. By inserting tuning rods of Plexiglas (6·4 mm long) into each cavity and varying its cavity length l the vortex whistle could be attenuated at any tuned frequency f_t. In order to reduce leakage, the intermediate section was covered by a sheath of Teflon and, furthermore, the entire test section was fastened by clamps.

With regard to the perforation on the main tube, holes of 1·2 mm in diameter were drilled out on the brass tube. In the initial arrangement, holes formed a staggered array, 45 rows in the circumferential direction and 25 in the axial direction. With the intermediate Teflon section fitted on the perforated tube, those holes on the tube that did not match with the acoustic cavities were identified and refilled with fibreglass filler in order to remove any unnecessary irregularity on the inner surface of the main tube. By this means, on the average a group of six holes upon the brass section matched with each acoustic cavity; over the main tube, the porosity became about 27 %.

These modifications, achieved after considerable trial and error, were found to suit our purpose: to reduce the vortex whistle as sharply as possible at the tuning frequency.

To ensure that the modification of the main tube from a smooth surface to a perforated one did not inadvertently alter the temperature separation, a test was run first with all cavity lengths set to zero. The results are shown in figure 8. Compared with the smooth tube, only the frequency was found to be noticeably affected, lowered by some 20 %, as might be expected from the slowdown of swirl due to the irregularity on the internal surface of the perforated tube. The cold temperature, measured at the coldest spot (position a of figure 7) was slightly higher for the perforated tube, and the sound level of the second harmonic slightly lower, but all in all they remained essentially unaffected; the peaks of the pure tones on the frequency spectra were as distinct and dominant as those for the smooth tube. Thus the perforated tube with zero acoustic cavity length still retained the characteristics of the smooth tube.

Next, the length of all the acoustic cavities was set to 1·02 cm and the thermocouple was left at the coldest spot. As the inlet pressure was slowly increased, the temperature at the cold spot kept on dropping, and at the same time both the frequency and intensity of the vortex whistle kept on increasing, as in the case of zero cavity – until, at $f = f_t = 4$ kHz, all of a sudden the sound became quieter, changing from a shrill whistle to a muffled hiss. At this instant, the cold temperature, which had gone down as low as -35 °C, immediately jumped up to 0·6 °C, with a temperature rise equal to 35·6 °C. The results are presented in figure 9, where, in addition to the temperature jump, the drops in the level of the first and second harmonics are shown. For the first harmonic, $\Delta\mathrm{dB}_1 = 25\,\mathrm{dB}$, for the second harmonic $\Delta\mathrm{dB}_2 = 14\,\mathrm{dB}$.

We display the successive change of frequency spectra around the present $f_t = 4{\cdot}0$ kHz in figure 10: (a) corresponds to $f = 3{\cdot}5$ kHz, below f_t, (b) $f = 3{\cdot}9$ kHz, just below f_t, (c) $f = f_t = 4{\cdot}0$ kHz, right at the tuned condition, and (d) $f = 4{\cdot}2$ kHz, above f_t. (The points corresponding to (a)–(d) appear in figure 9.) Comparison of the spectra clearly shows the following: the pure tones retained their spiky peaks right up to f_t (b); once $f = f_t$ (c), they suddenly became diminished and less distinct – 'spires' were lost. At the same time, the bases of the pure tones, as measured by the externally placed microphone, appear to become broadened ('haystacking'). Note also that between (b) and (c) the background noise level remained virtually the same.

As the frequency was increased further (*d*) the pure tone started to recover its spires. At the same time the cold temperature started to drop once again, as seen from figure 9.

We observe that at f_t the reduction of the sound level of the first harmonic, to whose frequency the cavity length was tuned, did cause the reduction in the second harmonic as well; this appears to add one more telling piece of evidence that the second harmonic is induced by the first harmonic. *Most importantly, the reduction of the first harmonic with* $m = 1$ *and its second harmonic did in fact reduce the temperature separation, as predicted by analysis.*

We cannot emphasize too strongly that the jump in temperature was not caused by any sudden change in the inlet temperature; the latter remained the same near f_t, before, after and in between, as is evident from the data shown in figure 9. Repeated tests confirmed that, once f approached f_t, just a slight increase in the upstream pressure precipitated the sudden reduction in noise level; or as was often the case, even when the upstream pressure was held constant, with f maintained equal to f_t, the precipitous drop in level took place spontaneously. Once the sound level became reduced and colder temperature shot up to a higher value, both stayed on that level until the upstream pressure was increased further.

Another phenomenon, compellingly evocative of the effect of acoustic streaming, could be easily perceived by sticking a finger near the exhaust: *below the tuning range, the flow discharging from the end of the main pipe was spiralling, outward and radially, over the end plate of figure* 7; *the region near the tube centreline was relatively quiescent – reminiscent of the eye of a hurricane. At the tuned condition, the swirling air suddenly rushed out along the tube centreline; the region over the end plate then became quieter.* This appears to bear vivid testimony to the expected *reversion* of the forced vortex to a Rankine vortex.

The data shown in figure 9 were taken with the cold-end thermocouple placed at the coldest spot (position *a* of figure 7). To confirm a point that the intrusion of the thermocouple did not inadvertently trigger the aforementioned sudden change, the thermocouple was withdrawn and placed flush with the cold-end plug (position *b*); then nothing lay in the way of the flow path. The results are shown in figure 11: at the same f_t as in figure 9 the sound level plummeted down again, accompanied by a temperature rise; the only major difference is the reduced amount of temperature jump, which corresponds to the higher temperature level at position *b*.

Figures 12 and 13 correspond to the cavity lengths of 1·52 and 2·03 cm, respectively; the cold-end thermocouple was placed at position *a* again. Other than the fact that f_t decreased as l increased, as expected, the basic features remained the same (the withdrawal of the thermocouple to position *a* again reproduced similar results).

Since the attenuation of the pure tone at f_t did not completely suppress the vortex whistle, as is evident from figure 10(*c*), by decreasing its intensity further it would appear possible to reduce the temperature separation further. In light of this – and although the temperature separation in the Ranque–Hilsch tube is not entirely attributable to the acoustic streaming induced by the vortex whistle, since the innermost core of any Rankine vortex must have total-temperature gradient caused by viscous stresses – it does not go too far to say that, for a vortex tube of uniflow type, the vortex whistle is in large part responsible for the Ranque–Hilsch effect.

An effort to obtain the radial distribution of temperature and pressure had to be

aborted, since the radial immersion of a probe into flow was itself found to cause severe interference with the measurements; a similar difficulty was also reported by Reynolds (1962). In this connection, a similar, repeatedly observed point is worthy of note: the excitation of the vortex whistle to a level sufficient for a significant degree of temperature separation depends strongly on the internal geometry of the tube. For example, in an experiment with a solid, non-perforated tube, a thermocouple of 3·2 mm diameter was axially inserted from the exhaust to a point near the tube entrance; at that axial location, as the thermocouple was being moved radially towards the tube periphery, suddenly the vortex whistle vanished, resulting in the reduction of temperature separation again. When the thermocouple was either retracted towards the centre or withdrawn axially, the sound re-emerged, accompanied by the recovery of temperature separation. The impression gained by this and other similar incidents, which include the aforementioned difficulty of the radial immersion of the probe, is that the vortex whistle is always latent, but a certain subtle change in the internal tube geometry either excites it to a sufficient level or fails to do so. Although any exhaustive investigation into this is beyond the scope of the present investigation, the following fact is highly suggestive: in the commercially available Ranque–Hilsch tube the internal surface of the tube is slightly tapered to form a short diffuser section near the entrance to the main pipe (for the performance of this see Takahama & Yokozawa 1981).

6. Concluding remarks

In sum, departing radically from previous theories, we have demonstrated through an analysis and experiments that the acoustic streaming caused by the vortex whistle, a spinning wave with a discrete frequency in swirling flows, is in great part responsible for the Ranque–Hilsch effect in the vortex tube of uniflow type: near the periphery of the tube, the induced 'd.c.' tangential velocity adds to the steady swirl, transforming the latter to a forced vortex and leading to the total-temperature separation in the radial direction.

To the extent that the temperature separation arises owing to the unsteadiness in flow, the present subject is the converse of the phenomena of Rijke tubes and thermally driven acoustic oscillations of liquid helium (e.g. Clement & Gaffney 1960), where the difference in the temperature gives rise to unsteady disturbances. In a broader context, to the extent that we seek in the present mechanism an organized origin distinct from the stochastic process, this falls under the same morphological group as the study of the large-scale structure in a mixing layer (Brown & Roshko 1974).

The author is indebted to Fr C. E. Danforth for calling his attention to the phenomenon of the annular cascade and its connection with the Ranque–Hilsch effect; to Messrs J. R. Goodman, J. Q. Chu and R. D. Fizer for their invaluable and indefatigable assistance in carrying out the experiments; to Mr H. R. Bankhead for his encouragement; to Mr H. Hehmann for his advice on the suppressor design; to Drs M. E. Goldstein and W. H. Heiser and Mr P. R. Gliebe for helping him to clarify several points by raising pertinent questions; to referees and Drs Caruthers and Maus for providing valuable comments on the original manuscript; to many other investigators on related subjects, for answering his various queries about their work. The work is supported by the Air Force Office of Scientific Research under contract no. F49620-78-C-0045.

Appendix

In this appendix, we obtain from (16) the frequency ω corresponding to the steady swirl prescribed in § 5.

For the radial profile given by (31), the boundary conditions for the unsteady disturbances are

$$\tilde{u}(r = r_0) = 0, \quad \tilde{p}, \tilde{u} \text{ continuous at } \quad r = r^*. \tag{A 1}$$

For a two-dimensional flow, Sozou & Swithenbank (1969) calculated the corresponding frequency relationship by a wholly numerical computation. (Although, as stated in § 4.1, the axial velocity is at present allowed to exist, as long as k is set equal to zero, w_0 drops out of (4) and the situation is the same as a two-dimensional flow.) Here we offer an approximate analytical representation, choosing $\tilde{\rho}$ as the primary dependent variable.

In the innermost core of the forced-vortex region defined by $0 < r < r^*$, we combine (16*a–f*) together and obtain the following single equation:

$$\frac{d^2\tilde{\rho}}{dr^2} + \left[\frac{1}{r} + \frac{(2\gamma-3)\,\Omega^2 r}{a_0^2(r)}\right]\frac{d\tilde{\rho}}{dr} + \left[\frac{2m\Omega^3}{\lambda_1 a_0^2(r)} + \frac{2(\gamma-2)\,\Omega^2}{a_0^2(r)} - \frac{m^2}{r^2} + \frac{D}{a_0^2(r)}\right]\tilde{\rho} = 0, \tag{A 2a}$$

where $a_0(r)$, λ_1, and D are given by

$$a_0^2(r) = a_0^2(r = r_0) + \tfrac{1}{2}(\gamma-1)\left[\Omega^2(r^2 - r^{*2}) - \Gamma^2\left(\frac{1}{r^{2*}} - \frac{1}{r_0^2}\right)\right], \tag{A 2b}$$

$$\lambda_1 = \Omega m - \omega, \tag{A 2c}$$

$$D = (\Omega m - \omega)^2 - 4\Omega^2, \tag{A 2d}$$

and $\tilde{u}$ is related to $\tilde{\rho}$ by

$$\tilde{u} = \frac{i}{\rho_0(r)\,D}\left\{\lambda_1 a_0^2(r)\frac{d\tilde{\rho}}{dr} + \tilde{\rho}\left[\frac{2ma_0^2(r)\,\Omega}{r} - (2-\gamma)\,\lambda_1 r\Omega^2\right]\right\}. \tag{A 2e}$$

On the other hand, in the free-vortex region defined by $r^* < r < r_0$, the governing equation is given by

$$\frac{d^2\tilde{\rho}}{dr^2} + \left[\frac{1}{r} + \frac{(2\gamma-3)\,\Gamma^2}{a_0^2(r)\,r^3} + \frac{4m\Gamma}{\lambda_2(r)\,r^3}\right]\frac{d\tilde{\rho}}{dr}$$
$$+ \left[\frac{\lambda_2^2(r)}{a_0^2(r)} - \frac{m^2}{r^2} + \frac{2m(2\gamma-3)\,\Gamma^3}{\lambda_2(r)\,r^6 a_0^2(r)} + \frac{8(m\Gamma)^2}{\lambda_2^2(r)\,r^6} - \frac{4m\Gamma}{\lambda_2(r)\,r^4} + \frac{2(2-\gamma)\,\Gamma^2}{a_0^2(r)\,r^4}\right]\tilde{\rho} = 0, \tag{A 3a}$$

where

$$a_0^2(r) = a_0^2(r = r_0) - \tfrac{1}{2}(\gamma-1)\,\Gamma^2\left(\frac{1}{r^2} - \frac{1}{r_0^2}\right), \tag{A 3b}$$

$$\lambda_2(r) = \frac{m\Gamma}{r^2} - \omega, \tag{A 3c}$$

and $\tilde{u}$ is related to $\tilde{\rho}$ by

$$\tilde{u} = \frac{i}{\rho_0(r)}\left\{\frac{a_0^2(r)}{\lambda_2(r)}\frac{d\tilde{\rho}}{dr} + \tilde{\rho}\left[\frac{2ma_0^2(r)\,\Gamma}{\lambda_2^2 r^3} - \frac{(2-\gamma)\,\Gamma^2}{\lambda_2 r^3}\right]\right\}. \tag{A 3d}$$

Equations (A 2*a*) and (A 3*a*) are the same as that obtained by Kerrebrock (1977).

We expand $\tilde{\rho}$, $\tilde{u}$ and ω in the power series of Ω:

$$\tilde{\rho} = \rho^{(0)} + \Omega\rho^{(1)} + \ldots, \tag{A 4a}$$

$$\tilde{u} = u^{(0)} + \Omega u^{(1)} + \ldots, \tag{A 4b}$$

$$\omega = \omega^{(0)} + \Omega\omega^{(1)} + \ldots . \tag{A 4c}$$

We confine our attention to $\omega^{(0)} = 0$, which corresponds to the lowest eigenvalue for the case without swirl. We substitute (A 4*a–c*) into the aforementioned governing equations for $\tilde{\rho}$ and retain the terms up to $O(\Omega)$. This yields the following expression for $\omega^{(1)}$:

$$\omega^{(1)} = \pm\,(|m| - 1 + \lambda^{-2|m|}), \tag{A 5a}$$

where $\lambda = r_0/r^*$, and ω becomes from (A 4*c*)

$$\omega = \pm\,(|m| - 1 + \lambda^{-2|m|})\,\Omega, \tag{A 5b}$$

where the + sign corresponds to $m > 0$, and the − sign to $m < 0$.

Sozou & Swithenbank (1969) list the computed values ω in their table 3; in our table 1, we compare their results with our analytical formula (A 5*b*), the latter being

$\frac{\Omega r^*}{a_0(0)}$	λ	$\omega r^*/a_0(0)\,m$				λ	$\omega r^*/a_0(0)\,m$			
		$m = 1$			$m = 2$		$m = 1$			$m = 2$
0·10	1·09	0·0841	(0·0841)	0·0854	(0·0854)	1·03	0·0942	(0·0942)	0·0944	(0·0944)
0·10	1·5	0·0444	(0·0444)	0·0598	(0·0598)	1·2	0·0694	(0·0694)	0·0741	(0·0741)
0·10	5	0·0040	(0·0040)	0·0050	(0·0050)	2	0·0250	(0·0250)	0·0531	(0·0531)
0·25	1·09	0·2099	(0·2104)	0·2132	(0·2135)	1·03	0·2353	(0·2356)	0·2359	(0·2361)
0·25	1·5	0·1105	(0·1111)	0·1490	(0·1497)	1·2	0·1729	(0·1736)	0·1848	(0·1852)
0·25	5	0·0100	(0·0100)	0·1246	(0·1252)	2	0·0622	(0·0625)	0·1321	(0·1328)
0·50	5	0·0199	(0·0200)	—	—	2	0·1222	(0·1250)	0·2603	(0·2656)
0·75	5	0·0296	(0·0300)	—	—	2	0·1807	(0·1875)	0·3814	(0·3984)
1·0	5	0·0392	(0·0400)	—	—	2	0·2367	(0·2500)	0·4941	(0·5312)

TABLE 1

shown in parentheses. The spaces left blank are unavailable from Sozou & Swithenbank's table. On the whole, our expression appears to be satisfactorily close to the numerical results, as long as the swirl Mach number, defined by them as $\Omega r^*/a_0(0)$, remains below 1.

REFERENCES

BATCHELOR, G. K. 1967 *An Introduction to Fluid Mechanics.* Cambridge University Press.

BATSON, J. L. & SFORZINI, R. H. 1970 *J. Spacecraft & Rocket* **7**, 159–163.

BROWN, G. L. & ROSHKO, A. 1974 *J. Fluid Mech.* **64**, 775–816.

BRUUN, H. H. 1969 *J. Mech. Engng Sci.* **11**, 567–582.

CHANAUD, R. C. 1963 *J. Acoust. Soc. Am.* **35**, 953–960.

CHANAUD, R. C. 1965 *J. Fluid Mech.* **21**, 111–127.

CLEMENT, J. R. & GAFFNEY, J. 1960 Thermal oscillations in low temperature apparatus. In *Advances in Cryogenic Engineering*, vol. 1 (ed. K. D. Timmerhaus), pp. 302–306. Plenum.

COLE, J. D. 1968 *Perturbation Methods in Applied Mathematics.* Blaisdell.

DEISSLER, R. G. & PERLMUTTER, M. 1960 *Int. J. Heat Mass Transfer* **1**, 173–191.

DUCK, P. W. & SMITH, F. T. 1979 *J. Fluid Mech.* **91**, 93–110.

FARADAY, M. 1831 *Phil. Trans. R. Soc. Lond.* **121**, 299–340.

GREENSPAN, H. P. 1968 *The Theory of Rotating Fluids*, p. 185. Cambridge University Press.

HADDON, E. W. & RILEY, N. 1979 *Q. J. Mech. Appl. Math.* **32**, 265–282.

HARTNETT, J. P. & ECKERT, E. R. G. 1957 *Trans. A.S.M.E.* **79**, 751–758.

HILSCH, R. 1947 *Rev. Sci. Instrum.* **18**, 108–113.

KELVIN, LORD 1880 *Phil. Mag.* **5**, 155–168.

KENDALL, J. M. 1962 Experimental study of a compressible viscous vortex. *Tech. Rep.* no. 32-290. *JPL, Calif. Inst. of Tech.*

KERREBROCK, J. L. 1977 *A.I.A.A. J.* **15**, 794–803.

KNOERNSCHILD, E. 1948 Friction laws and energy transfer in circular flow, part II. Energy transfer in circular flow and possible applications (explanation of the Hilsch or Ranque effect). *Tech. Rep.* F-TR-2198-ND, GS – USAF; *Wright Patterson Air Force Base* no. 78.

KUROSAKA, M. 1980 *U.S. Air Force Office of Scientific Research Rep.* AFOSR-TR-80-0509.

LAY, J. E. 1959 *Trans. A.S.M.E.*, C, *J. Heat Transfer* **81**, 202–212.

LIGHTHILL, M. J. 1978*a* *J. Sound Vib.* **61**, 391–418.

LIGHTHILL, M. J. 1978*b* *Waves in Fluids*, p. 347. Cambridge University Press.

LINDERSTRØM-LANG, C. U. 1971 *J. Fluid Mech.* **45**, 161–187.

MCGEE, R. 1950 *Refrig. Engng* **58**, 974–975.

RAGSDALE, R. G. 1961 *NASA TN* D-1051.

RAKOWSKI, W. J. & ELLIS, D. H. 1978 Experimental analysis of blade instability, vol. 1. R78 AEG 275, *General Electric Company Rep. for* F 33615-76-C-2035, *to Air Force Aero Propulsion Lab.* WPAFB. 67–71.

RAKOWSKI, W. J., ELLIS, D. H. & BANKHEAD, H. R. 1978 *A.I.A.A. Paper* no. 78-1089.

RANQUE, G. J. 1933 *J. Phys. Radium* **4**, 112S–115S.

RAYLEIGH, LORD 1884 *Phil. Trans. R. Soc. Lond.* **175**, 1–21.

REYNOLDS, A. 1962 *J. Fluid Mech.* **14**, 18–20.

RILEY, N. 1967 *J. Inst. Maths. Applics* **3**, 419–434.

SAVINO, J. M. & RAGSDALE, R. G. 1961 *Trans. A.S.M.E.* C, *J. Heat Transfer* **83**, 33–38.

SCHELLER, W. A. & BROWN, G. M. 1957 *Ind. Engng Chem.* **49**, 1013–1016.

SCHEPPER, G. W. 1951 *Refrig. Engng* **59**, 985–989.

SECOMB, T. W. 1978 *J. Fluid Mech.* **88**, 273–288.

SIBULKIN, M. 1962 *J. Fluid Mech.* **12**, 269–293.

SOZOU, C. & SWITHENBANK, J. 1969 *J. Fluid Mech.* **38**, 657–671.

SPRENGER, H. 1951 *Z. angew. Math. Phys.* **2**, 293–300.

SPRENGER, H. 1954 Über thermische Effekte in Resonanzrohren. *Mitt. Int. Aerodyn. ETH, Zürich*, Nr. 21, p. 18.

STUART, J. T. 1963 Unsteady boundary layers. In *Laminar Boundary Layers* (ed. by L. Rosenhead), chap. 7, p. 384. Oxford University Press.

STUART, J. T. 1966 *J. Fluid Mech.* **24**, 673–687.

SYRED, N. & BEÉR, J. M. 1972 In *Proc. 2nd Int. J.S.M.E. Symp. on Fluid Machinery, Tokyo*, vol. 2, pp. 111–120.

TAKAHAMA, H. 1965 *Bull. J.S.M.E.* **8**, 433–440.

TAKAHAMA, H. & YOKOZAWA, H. 1981 *J. J.S.M.E.* **84**, 651–656 (in Japanese).

VAN DEEMTER, J. J. 1952 *Appl. Sci. Res.* A **3**, 174–196.

VAN DYKE, M. 1962*a* Second-order compressible boundary layer theory with application to blunt bodies in hypersonic flow. In *Hypersonic Flow Research* (ed. F. R. Riddle), pp. 37–75. Academic.

VAN DYKE, M. 1962*b* *J. Fluid Mech.* **14**, 161–177.

VAN DYKE, M. 1969 Higher-order boundary layer theory. In *Ann. Rev. Fluid Mech.* **1**, 265–292.

VONNEGUT, B. 1950 *Rev. Sci. Instrum.* **21**, 136–141.

VONNEGUT, B. 1954 *J. Acoust. Soc. Am.* **26**, 18–20.